BIOPROBES 54

INVITROGEN CELLULAR ANALYSIS

OCTOBER 2007

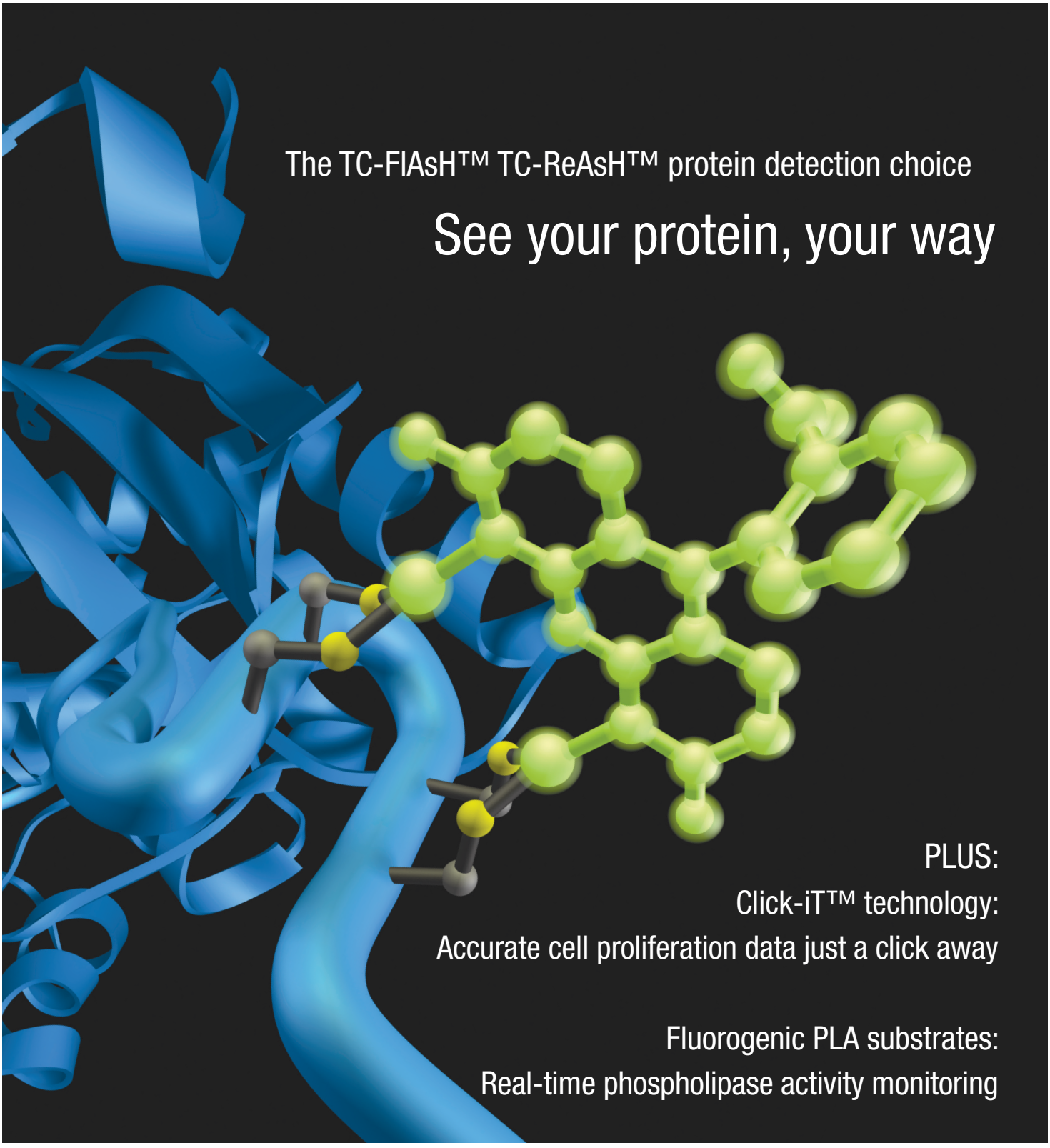

invitrogen™

Molecular Probes®
invitrogen detection technologies

Published by Invitrogen
Eugene, Oregon USA © 2007

BioProbes® newsletter is published several times each year. *BioProbes* is dedicated to furnishing researchers with the very latest information about cellular analysis products and their applications. For a listing of our products, along with extensive descriptions and literature references, please see our website. Prices are subject to change without notice. Quantity discounts may be available.

Editors
Jennifer Bordun
Coleen Miller, Ph.D.

Contributing Editors
Jay Gregory, Ph.D.
Robyn Leung, M.S.
Grace Richter, Ph.D.

Contributing Writers
Sheetal Bhakta, M.S.
Hans Beernink, Ph.D.
Chris Brotski
Beth Browne, Ph.D.
Stephen Chamberlain, Ph.D.
Ian Dimmick
Kathleen Free
William Godfrey, Ph.D.
Thao Hoang, Ph.D.
Mike Ignatius, Ph.D.
Taryn Jackson, Ph.D.
Iain Johnson, Ph.D.
Magnus Persmark, Ph.D.

Design
Lynn Soderberg

Cover Design
Kelly Christensen

Figures and Images
Robert Batchelor, M.S.
Wei R. Chen
Ian Dimmick
George Hanson, Ph.D.
Dani Hill
Thao Hoang, Ph.D.
Lydia Jablonski
Shin Nagayama
Michael O'Grady, M.S.
Bethany Sutton, M.S.
Yu-Zhong Zhang, Ph.D.

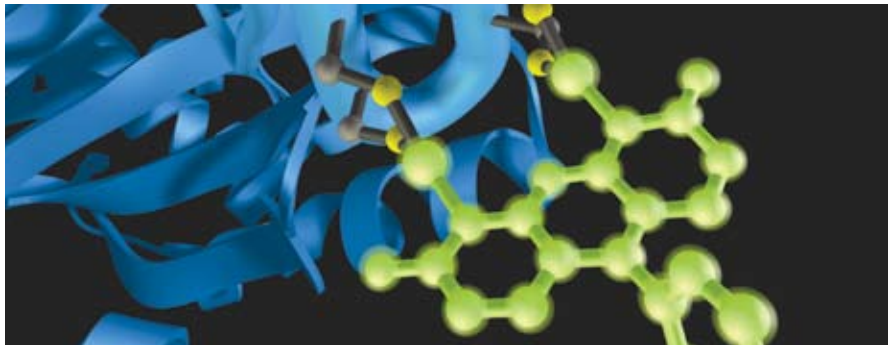

BioProbes 54

Features

Departments

New sections in *BioProbes* make it easier to find the articles you want to read

NEW TECHNOLOGIES—learn the basics about the newest products to come out of our laboratories

PRACTICAL APPLICATIONS—get in-depth information, including data from other researchers, about products you haven't tried

DEPARTMENTS—find out about the newest web tools and published papers, get a first look at our newest products, enjoy articles written by our readers, and more

The use of Qdot® nanocrystals in flow cytometry

NOVEL REAGENTS EXPAND THE SCOPE OF MULTICOLOUR PANELS.

Qdot® nanocrystals provide an exciting new array of fluors for use in flow cytometry. The capabilities of flow cytometry instrumentation are continually expanding; currently we can distinguish up to 18 fluorescent colours on or in the cells of interest. To take advantage of this capability and implement a multicolour approach, we need an appropriate range of antibodies conjugated with fluorochromes that are spectrally distinct. Unfortunately, some of the most interesting markers to us are only available in a limited range of conjugates. Often, we have to resort to indirect staining protocols to label cellular antigens with fluorochromes of choice. Given this, my lab has been looking at expanding our fluorochrome palette by using biotinylated primary antibodies and streptavidin conjugated to Qdot® nanocrystals. The decision to look objectively at the nanoparticles, Qdot® nanocrystals, was made for three main reasons:

1. Streptavidin conjugates of Qdot® nanocrystals are available in a wide range of colours
2. Qdot® nanocrystals can be excited by almost any laser; with careful use, this is a distinct advantage
3. Extinction coefficients and quantum yields of Qdot® nanocrystals are very high compared with those of standard fluorochromes, making these reagents potentially very useful for resolving populations with weak antigen expression

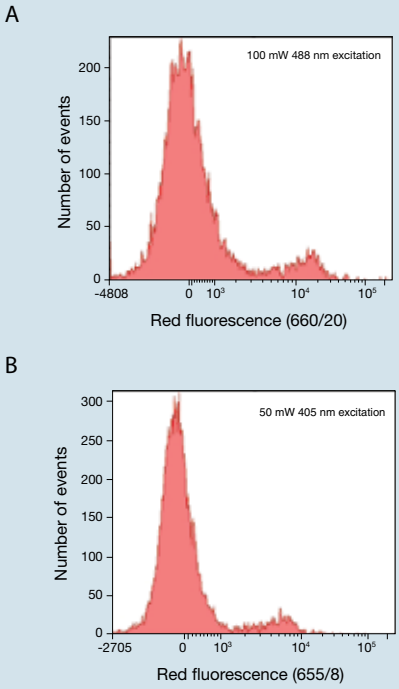

Figure 1—Human peripheral blood lymphocytes stained with biotin–anti-CD19 and Qdot® 655–streptavidin. The lymphocyte population was analysed simultaneously in both channels on a BD FACSAria™ flow cytometer using excitation with a 100 mW 488 nm laser (A) and 50 mW 405 nm laser (B), using 660/20 and 655/8 bandpass filters, respectively.

Table 1—Extinction coefficient of Qdot® streptavidin conjugates at common excitation wavelengths, in $cm^{-1}M^{-1}$. For comparison, the extinction coefficient of fluorescein with 488 nm excitation is ~80,000 $cm^{-1}M^{-1}$.

Product	350 nm	405 nm	488 nm	532 nm
Qdot® 525 nanocrystals	710,000	360,000	130,000	NA
Qdot® 565 nanocrystals	1,900,000	1,100,000	290,000	139,000
Qdot® 585 nanocrystals	3,500,000	2,200,000	530,000	305,000
Qdot® 605 nanocrystals	4,400,000	2,800,000	1,100,000	580,000
Qdot® 655 nanocrystals	9,100,000	5,700,000	2,900,000	2,100,000
Qdot® 705 nanocrystals	12,900,000	8,300,000	3,000,000	2,100,000
Qdot® 800 nanocrystals	12,600,000	8,000,000	3,000,000	2,000,000

NA = Not applicable.

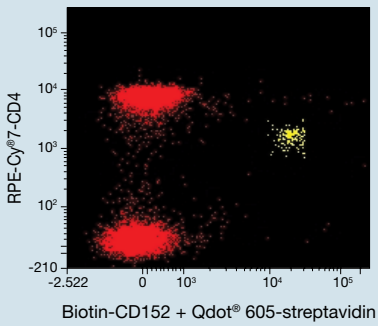

Figure 2—Human peripheral blood lymphocytes stained with anti-CD4–RPE-Cy®7 and biotin–anti-CD152 with Qdot® 605 streptavidin. The sample was analysed using a BD FACSAria™ flow cytometer with 488 nm excitation using a 780/60 filter for RPE-Cy®7 and a 610/20 filter for Qdot® 605 nanocrystals.

Qdot® nanocrystals demonstrate increasing excitation efficiency with decreasing wavelength of excitation, as seen with the extinction coefficient values in Table 1. This means that Qdot® nanocrystals will excite very well with UV or violet light, but they can also be used with longer-wavelength excitation sources in combination with organic or phycobiliprotein fluorochromes. One example is shown in Figure 1, where Qdot® 655 nanocrystal–labelled CD19-positive cells fluoresce brightly with excitation from a 100 mW 488 nm laser and with a 50 mW 405 nm laser.

Qdot® nanocrystal secondary reagents can be easily dropped into multicolour immunofluorescence protocols; this is particularly true of the Qdot® streptavidin reagents. We wanted fluorochromes that were very bright in relation to other commonly used fluorochromes such as fluorescein and even R-phycoerythrin (RPE). We also needed fluorochromes that would be easy to use with biotinylated antibodies and that fit the emission filters of our customised BD FACSAria™ flow cytometer (BD Biosciences, filter configuration in Figure 4).

Figure 2 shows dual staining of human leukocytes for CD4 and CD152. The Qdot® staining allowed outstanding resolution of the small CD152-positive population. Figure 3 shows how a quantum dot reagent can fit into a nine-colour panel. In this case, Qdot® nanocrystals were used to resolve a very small population of B cells within normal lymphoid cells. The nine-colour panel also allowed resolution of CD3- and CD7-positive cells, of interest as a differential T cell maturation marker with CD2, whilst excluding dead cells and monocytes by propidium iodide and CD14, respectively.

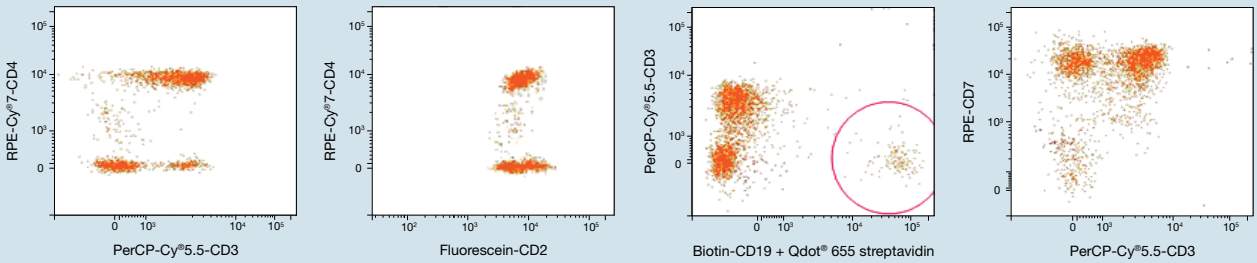

Figure 3—A nine-colour experiment using Qdot® 655 and an extended incubation time for the antibodies to optimise the detection of CD19 expression. Human peripheral blood cells were analysed using a BD FACSAria™ flow cytometer using 405 nm and 488 nm excitation. Lymphocytes were gated using side scatter and CD45; monocytes and dead cells were excluded with CD14 and propidium iodide, respectively. This enabled us to look at viable cells, which were free from monocyte contamination. CD19 was evaluated using Qdot® nanocrystals primarily, as we had experienced low expression of this marker which seemed to be both fluorochrome- and patient-specific. The $CD3^{+}CD7^{+}$ population was also of interest as a differential T cell maturation marker with CD2 and CD3.

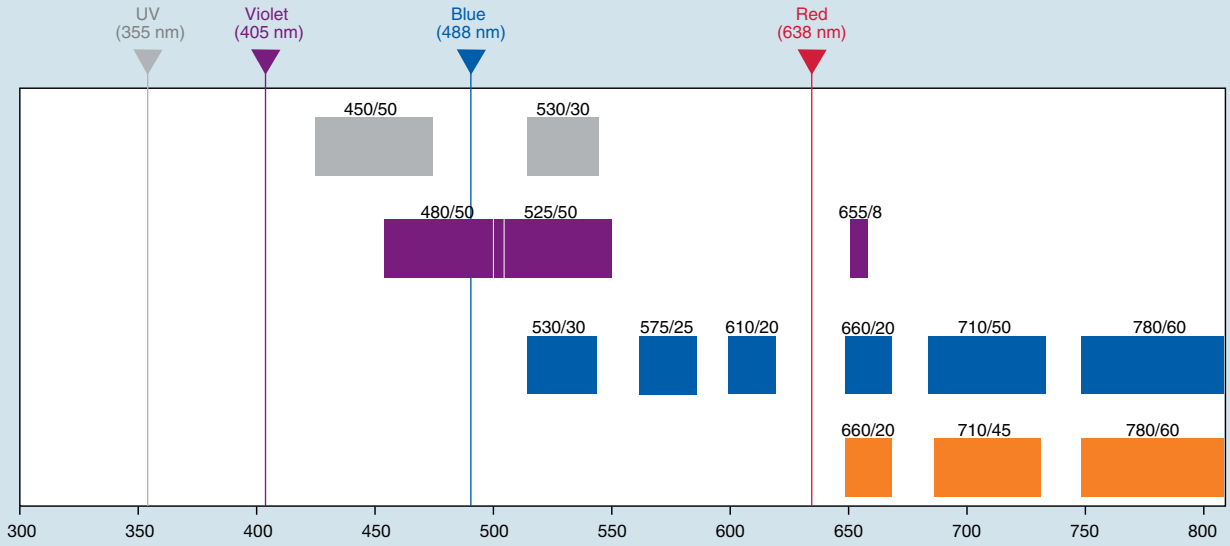

Figure 4—Diagram used to illustrate potential Qdot® overlaps between channels with respect to excitation from different lasers.

We were particularly pleased that we did not have to purchase additional filter sets to use Qdot® nanocrystals with our FACSAria™ instrument. To quantify spectral overlap, we have tested Qdot® nanocrystals with the same protocol employed for all new fluorochromes used within the core facility. Briefly, compensation beads were labelled with a primary antibody, which was in turn labelled with a streptavidin Qdot® nanocrystal. These beads were then analysed under standard lymphocyte settings for each laser, and spectral overlap was observed. We found that the overlap was satisfactory and, in many cases, reduced when compared to the more conventional fluorochromes. It should be remembered, however, that because Qdot® nanocrystals are excited by all lasers, emission will be detected by multiple PMTs if there is any duplication of absorption filters amongst the multiple-laser excitation. Figure 4 shows a diagram that I find very useful for all fluorochromes, including Qdot® nanocrystals. This chart outlines the configuration of our FACSAria™ instrument. Using this chart, we can see that, for example, the Qdot® 655 nanocrystal could be detected by three photomultiplier tubes, whereas the Qdot® 605 nanocrystal will be detected by only one.

I feel that Qdot® nanocrystals are very useful tools for researchers who use multicolour flow cytometry and who want to easily drop in an additional fluorochrome or better resolve dimly expressed antigens. Qdot® nanocrystals, however, do have to be used intelligently—users have to be aware of the potential need to compensate across lasers due to the multiple-laser absorption properties of the Qdot® nanocrystals. The multiple-laser excitation also acts as a beneficial characteristic, allowing their substitution for potentially troublesome tandem conjugates. Through analysis of the emission channels on your flow cytometer with a tool similar to the one shown in Figure 4, you should be able to find channels that will easily accommodate the use of Qdot® nanocrystal conjugates. ■

Article contributed by Ian Dimmick, Flow Cytometry Core Facility Manager, North East England Stem Cell Institute, Bioscience Centre, International Centre for Life, Newcastle Upon Tyne, Great Britain.

ORGANELLE LIGHTS™ CELLULAR LANDMARKS

Organelle Lights™ reagents are fluorescent protein (FP)–signal peptide fusions designed to traffic to specific cellular compartments (organelles and subcellular structures). The FP genes are cloned into a baculovirus chromosome and packaged in viral particles for highly efficient cellular delivery via proven BacMam technology. Transduction is efficient and reproducible in most cell lines—including primary and stem cells—without apparent cytopathic effects.

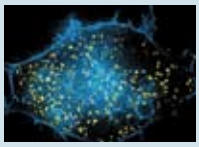

- Free yourself from making your own constructs and transfection complexes—well-characterized, targeted, safe, and easy-to-use fluorescent protein intracellular landmarks
- Multiplex easily with other Organelle Lights™ constructs, fluorescent organic dyes, or Qdot® conjugates
- Study dynamic cellular processes and use for subcellular colocalization experiments with precise spatial and temporal resolution

Visit **www.invitrogen.com/olights** to learn more about Organelle Lights™ reagents.

CLICK-IT™ EdU—FREE EdU-CATION

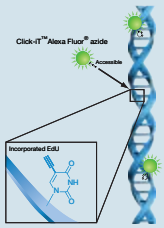

If you haven't already heard, you may want to "click" soon to learn about one of the most powerful technologies to hit life science research—click chemistry. Discover how it has been applied and has revolutionized cell proliferation assays. Visit **www.invitrogen.com/edu** today.

PHAGOCYTOSIS WITH PHRODO™ DYE

The new Molecular Probes® proprietary pH-sensitive rhodamine-based pHrodo™ dye is a specific sensor of phagocytic events. When conjugated to microorganisms, pHrodo™ dye provides you with a superior tool to distinguish phagocytic events from nonspecific binding to cells.

pHrodo™ pH-sensitive dye:

- Nonfluorescent at neutral pH, bright red in acidic environments
- Multiplex with green dyes such as FITC, Alexa Fluor® 488, GFP, fluo-4, or calcein
- Label microorganisms or proteins of choice

pHrodo™ BioParticles® conjugates:

- Detect phagocytosis and endocytosis and easily discriminate endocytosed from adherent and extracellular particles
- No need for wash steps or quencher dye
- Ready for imaging and flow cytometry

Please visit our web page dedicated to this new and exciting technology: **www.invitrogen.com/phrodo**.

PRODUCTS FOR MICROBIOLOGY RESEARCH

The Microbiology web page offers a convenient, categorized listing of fluorescence-based products used to study microorganisms, as developed by Invitrogen or as reported in published scientific literature. The page features fluorescent stains for microbial detection, counting, viability and vitality, and Gram character determination for various analytical platforms such as microscopy, fluorometry, and flow cytometry. Included are links to searchable catalogs, the Molecular Probes Handbook, assay protocols, a link to Howard M. Shapiro's Practical Flow *Cytometry, 4th Edition*, and recent poster presentations. Updates are added often, so why not bookmark the Microbiology web page (**probes.invitrogen.com/products/microbiology**).

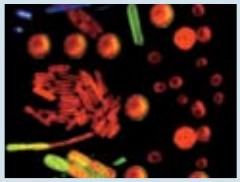

BIOPROBES EXTRA

From cover to cover, we squeeze as much information into every issue of *BioProbes* as space will allow. Now we're making even more articles available to you in the form of *BioProbes Extra* articles. These PDF documents contain bookmarks, active hyperlinks, and fully searchable text, making it easy to get to the information and products you're interested in. Find the *BioProbes Extra* articles at **www.invitrogen.com/bioprobes**. Check out this month's articles:

- Tools for Akt/PKB signaling pathway analysis: Phosphorylation site–specific antibodies
- See phagocytosis in a new light: pHrodo™ phagocytosis kits for flow cytometry

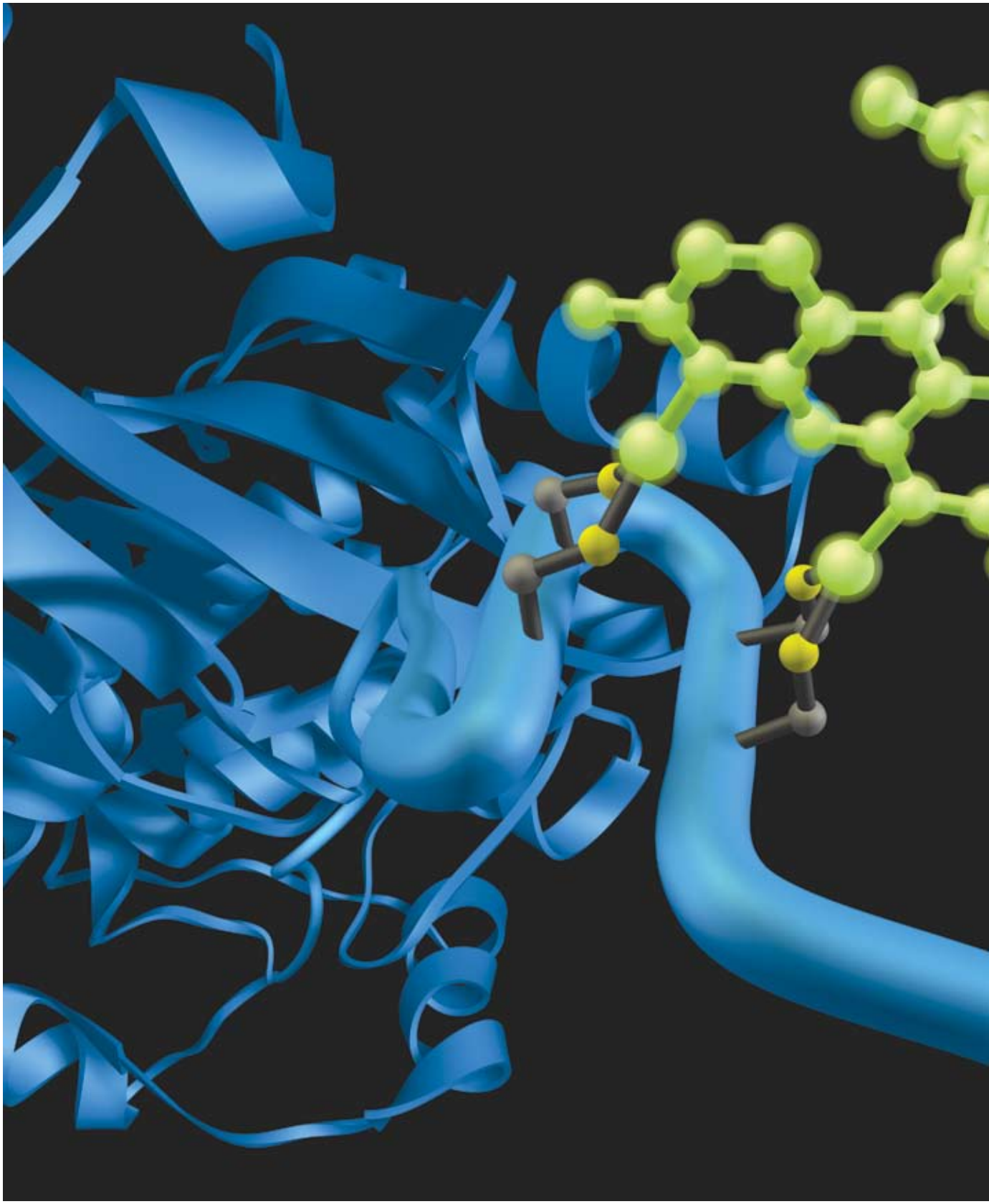

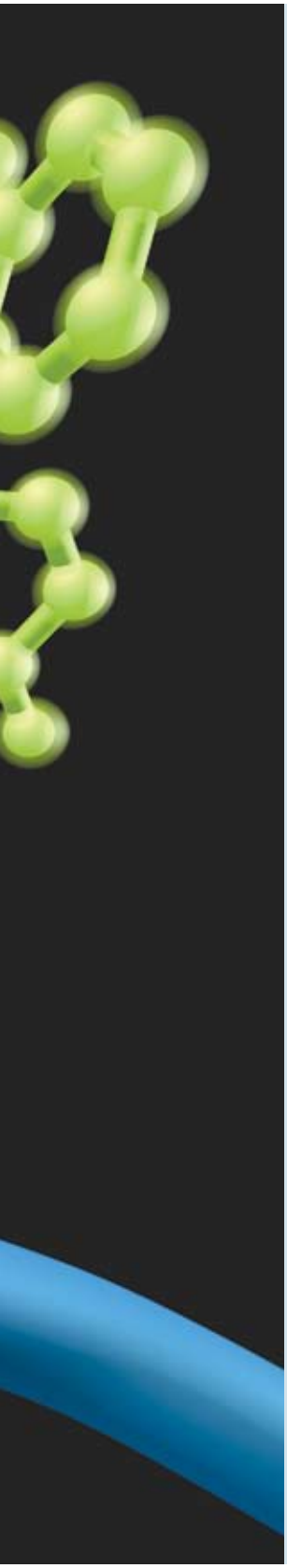

The TC-FlAsH™ TC-ReAsH™ protein detection choice

SEE YOUR PROTEIN, YOUR WAY.

How much time and effort would you save if one label worked for multiple detection methods? With the TC-FlAsH™ TC-ReAsH™ tetracysteine (TC) reagents, you don't have to wonder anymore. Using a unique, six-amino-acid sequence and easy-to-follow protocols, you can label your protein once and then use it in live-cell imaging and in-gel expression analysis experiments. The TC-FlAsH™ TC-ReAsH™ detection technology, based on the TC tag first described by Roger Tsien and colleagues,[1] works through the high-affinity interaction of a biarsenical molecule (contained in the FlAsH and ReAsH reagents) with thiols (contained in the TC tag coexpressed with the protein of interest). With this single approach, you can perform live-cell imaging, in-gel expression analysis, and purification studies on your protein of interest. →

Figure 1—Illustration of FlAsH binding to the TC tag.

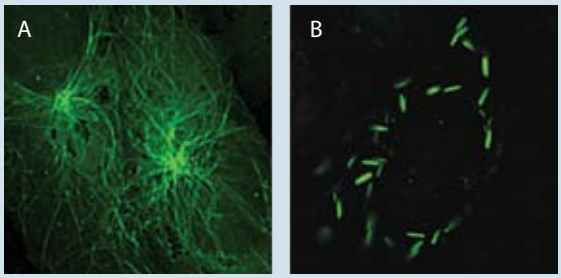

Figure 2—CHO-K1 cells expressing a tetracysteine-tagged version of β-tubulin, labeled with TC-ReAsH™ reagent. Upon treatment with vinblastine, a compound known to perturb cytoskeletal structure, tubulin drastically rearranges from a reticular structure (A) to rod shapes (B).

One tag expands your visualization options

FlAsH reagent is a biarsenical molecule based on modification of fluorescein to contain two arsenic atoms (Figure 1), while ReAsH reagent is a similarly modified resorufin. Virtually nonfluorescent by themselves, these reagents become highly fluorescent when bound to the thiol-containing TC tag (Cys-Cys-Xaa-Xaa-Cys-Cys, where Xaa-Xaa is typically Pro-Gly).[2]

Transfecting the host cell line with an expression construct incorporating the protein of interest fused to a TC tag (CCPGCC) is the first step to accessing the TC-FlAsH™ TC-ReAsH™ technology. Because it's so small, this six-amino-acid tag is unlikely to disrupt native protein structure and function. When the FlAsH or ReAsH reagent is added, it binds to the tetracysteine motif and becomes fluorescent. Using the appropriate FlAsH or ReAsH reagent, the tagged protein can then be imaged with a TC-FlAsH™ or TC-ReAsH™ In-Cell Detection Kit or be detected in a polyacrylamide gel with the TC-FlAsH™ Expression Analysis Detection Kit.

Vivid in-cell detection

FlAsH and ReAsH are both cell-permeant reagents. Therefore, TC-tagged proteins can be fluorescently labeled and tracked in live mammalian cells. Simply add the FlAsH (for green fluorescence) or ReAsH (for red fluorescence) reagent to cells expressing a TC-tagged protein (Figure 2). Live-cell applications with the TC-FlAsH™ and TC-ReAsH™ In-Cell Tetracysteine Detection Kits include protein localization and trafficking, pulse chase, FRET, protein–protein interaction, protein turnover, receptor activation, and fluorophore-assisted light inactivation (see **probes.invitrogen.com/lit/bioprobes52** and **www.invitrogen.com/flashreash** for a list of references).

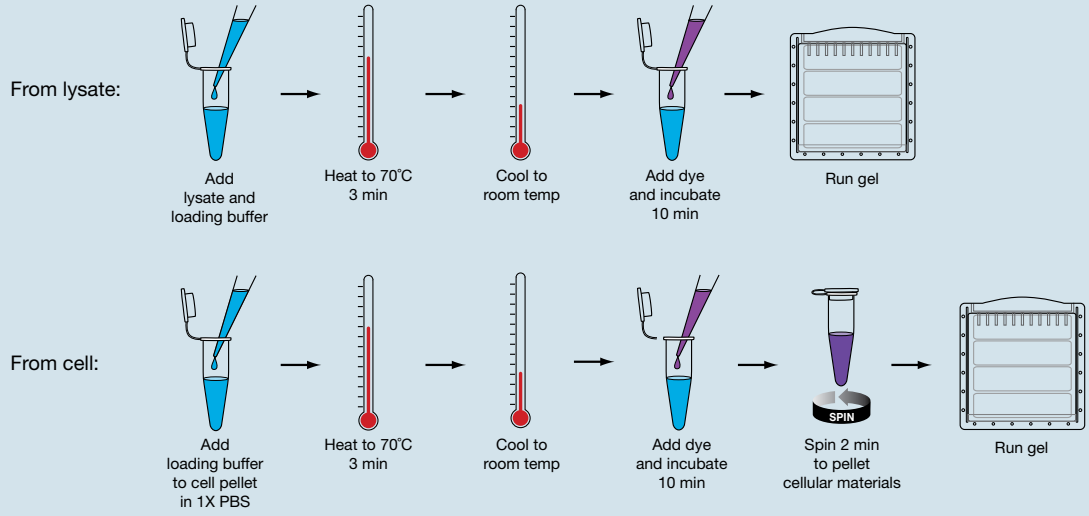

Figure 3—Workflow used to prelabel proteins before SDS-PAGE.

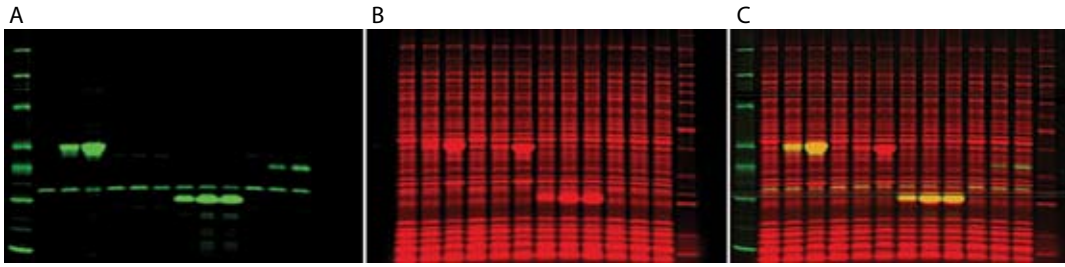

Figure 4—Immediate results obtained using TC-FlAsH™ Expression Analysis Detection Kit. TC-tagged proteins label with FlAsH and fluoresce green (A), total proteins are labeled with a red dye (B), and the overlay image reveals relative amounts of protein (C).

Expression analysis detection

Traditional methods for detecting protein expression involve labor-intensive post-staining with Coomassie®, silver, or fluorescent stains or western blotting. These messy, time-consuming, and often finicky procedures can be replaced with a quick, clean, and tag-specific procedure using the TC-FlAsH™ Expression Analysis Detection Kit—Red or Orange. Simply heat the cellular lysate or purified TC-tagged protein in loading buffer, incubate for ten minutes at room temperature with an optional total-protein stain, and then load, run, and image the gel (Figure 3). The resulting bands are sharp and clear with no background (Figures 4A and 4B). There is no need to post-stain, fix gels, transfer gels to membranes, or obtain antibodies for western blot, saving significant time and effort. Furthermore, the risk of tearing gels and subsequently losing data is greatly reduced, as are the amount of chemical waste and the mess of post-staining procedures. Lastly, the ability to perform a western blot after in-gel detection is not lost, as antibodies are unaffected by the FlAsH and total-protein stains.

In addition, the FlAsH and total-protein stains display a linear relationship between fluorescence intensity and protein concentration, enabling the determination of protein concentration when compared to standards in the same gel (Figure 4C). The sensitivity of the TC-FlAsH™ Expression Analysis Detection Kit is excellent. As little as 14 fmol (250 pg/band of an 18 kDa protein) when imaged out of cassette and 220 fmol (4 ng/band of an 18 kDa protein) when imaged on a NuPAGE® Novex® 4–12% Gel can be detected (sensitivity can vary by cassette type).

Two-in-one technology

One tag really does offer the detection options you need. Whether you are looking for exceptionally sensitive fluorogenic detection, in-gel protein visualization with western blot–like results, or both, you can achieve your goals with the Molecular Probes® TC-FlAsH™ and TC-ReAsH™ reagents.

Learn more about TC-FlAsH™ and TC-ReAsH™ TC tag detection at **www.invitrogen.com/flashreash.** ■

References

1. Griffin, B.A. et al. (1998) *Science* 281:269–272.
2. Adams, S.R. et al. (2002) *J Am Chem Soc* 124:6063–6076.

Products	Quantity	Cat. no.
TC-FlAsH™ II In-cell Tetracysteine Tag Detection Kit, green fluorescence, for live-cell imaging	1 kit	T34561
TC-ReAsH™ II In-cell Tetracysteine Tag Detection Kit, red fluorescence, for live-cell imaging	1 kit	T34562
TC-FlAsH™ TC-ReAsH™ II In-cell Tetracysteine Tag Detection Kit, with mammalian TC-Tag Gateway® expression vectors, green and red fluorescence, for live-cell imaging	1 kit	T34563
TC-FlAsH™ Expression Analysis Detection Kit—Orange, fluorescent in-gel detection of TC-tagged and total protein	1 kit	A10067
TC-FlAsH™ Expression Analysis Detection Kit—Red, fluorescent in-gel detection of TC-tagged and total protein	1 kit	A10068

Improved results are just a click away

ACCURATE CELL PROLIFERATION DATA WITH CLICK-iT™ EdU.

Understanding how and why an assay works is sometimes essential to getting the best results and interpreting those results correctly. Sometimes it can be very informative to question the assay—does this really accomplish what I'm trying to achieve? Is there a better way? For the past 20 years, the modified nucleoside bromodeoxyuridine (BrdU) has been a mainstay in assays designed to monitor cell proliferation by examining new DNA synthesis. But how does it really work? More importantly, how might it be affecting your sample? It may be time to consider Click-iT™ EdU assays, which offer significant advantages over current methodologies.

Accurately measures the proliferation of individual cells

Many cell proliferation assays promise accuracy; the question is, do they actually deliver? At the individual cell level, accurate cell proliferation measures new DNA synthesis (Figure 1). Assays that measure redox potential (alamarBlue®, MTT, WST-1) or ATP indirectly quantitate proliferating cells of an entire cell population; differences between individual cells cannot be measured from the available readout. Reagents that measure DNA content, including DAPI and the CyQUANT® assays, are more accurate, but they are still only capable of measuring proliferation of the total cell population—differences between individual cells will go undetected. CFSE measures cell population division. Cell cycle stains (propidium iodide, Vybrant® DyeCycle™ stains) are capable of measuring new DNA synthesis of individual cells, but mathematical models are required to calculate proliferating cells. These stains work well in simple cases, but with complex populations, including populations with polyploidy, the accuracy of this measurement decreases. This leaves reagents that directly measure new DNA synthesis at the single-cell level. Initially this was achieved by the incorporation of a radioactive nucleoside, ^{3}H-thymidine, a method that was replaced by antibody-based detection of the nucleoside analog bromodeoxyuridine (BrdU). The Click-iT™ EdU assays use the nucleoside analog EdU (5-ethynyl-2′-deoxyuridine). Cell proliferation of individual cells can be accurately measured through the detection of incorporation of either EdU or BrdU.

Compatible with a variety of instruments and samples

An additional advantage to the BrdU- and EdU-based assays is that they offer flexible readout and can be used either with cells or *in vivo*. These assays can be optimized for use on any instrument platform, including flow cytometers, high-throughput imaging (HCS), and standard microscopes. These assays can also be used with adherent or suspension cells or even injected into animals for subsequent analysis by imaging or flow cytometry.

Easy to perform

Both the Click-iT™ EdU and BrdU assays follow similarly simple workflows. Cells are first fed the nucleoside analog, allowed to proliferate, then fixed and permeabilized, followed by detection and analysis of the incorporated nucleoside. Where EdU and BrdU methods differ is in their simplicity of detection (Figure 2); detection of EdU is based on a click reaction—a copper-catalyzed covalent reaction between an azide and an alkyne. In this reaction, the EdU contains the alkyne, and either an Alexa Fluor® dye or Pacific Blue™ dye contains the azide. The small size of the dye azide allows for efficient detection of the incorporated EdU under mild conditions. Standard aldehyde-based fixation and detergent permeabilization are sufficient for the Click-iT™ detection reagent to gain access to the DNA. This is in contrast to the BrdU assays that require DNA denaturation (using HCl, heat, or DNase) to expose the BrdU so that it may be detected with an anti-BrdU antibody.

Multiplex capability

By eliminating the requirement for DNA denaturation, additional targets can be easily and reliably investigated. DNA denaturation protocols using 4N HCl and methanol can affect cell morphology and antigen recognition sites. Although milder than HCl, DNase denaturation can destroy the ability to perform cell cycle analysis. Finding that balance between DNA that is sufficiently denatured for anti-BrdU access, but still retaining sufficient amounts of dsDNA for the cell cycle dye to bind, is difficult. With Click-iT™ EdU, content-rich results are now truly easy to obtain. You can not only accurately measure proliferation of individual cells, but also simultaneously detect cell cycle, intracellular, and extracellular targets. It is important to note that the copper catalyst of the click reaction can affect the fluorescence of other molecules; adjustments to some existing protocols may be necessary (Table 1). The combination of Click-iT™ EdU's advantages—simplicity, accuracy, compatibility, and reliability—will be worth these efforts.

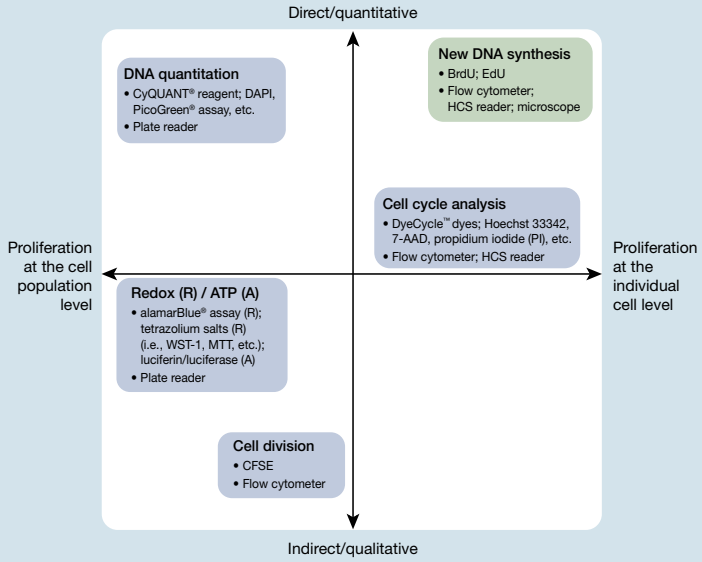

Figure 1—Comparison of various assays for cell proliferation. (The top line indicates the general method, the second line lists examples of products, and the third line lists instrument platforms.)

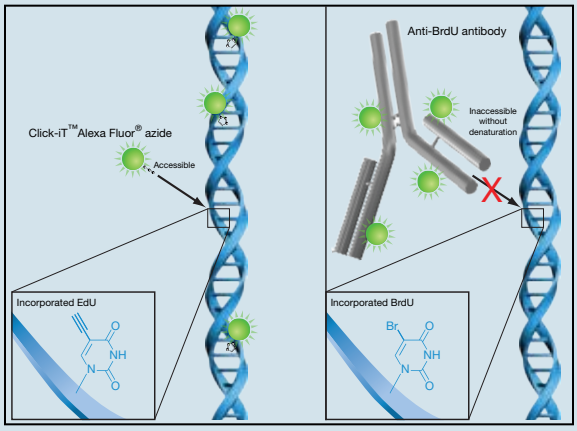

Figure 2—Detection of the incorporated EdU with the Alexa Fluor® azide versus incorporated BrdU with an anti-BrdU antibody. The small size of the Alexa Fluor® azide eliminates the need to denature the DNA in order for the detection reagent to gain access to the nucleoside.

Table 1—Click-iT™ EdU compatibility.*

Fluorescent molecules	Notes
Qdot® nanocrystals	Use Qdot® nanocrystals after the Click-iT™ detection reaction
Fluorescent proteins (GFP)	Use organic dye–based reagents to detect protein expression
Organic dyes (i.e., Alexa Fluor® dyes, fluorescein (FITC))	These fluorescent molecules are completely compatible with Click-iT™ EdU
PerCP, allophycocyanin (APC), and APC-based tandems (i.e., Alexa Fluor® 680-APC)	These fluorescent molecules are completely compatible with Click-iT™ EdU
R-phycoerythrin (RPE) and RPE-based tandems (i.e., Alexa Fluor® 610-RPE)	Use these RPE and RPE-based tandems after the Click-iT™ detection reaction

*Compatibility indicates whether the fluorescent molecule itself or the detection methods involve components that are unstable in the presence of the copper catalyst used for the Click-iT™ EdU detection reaction.

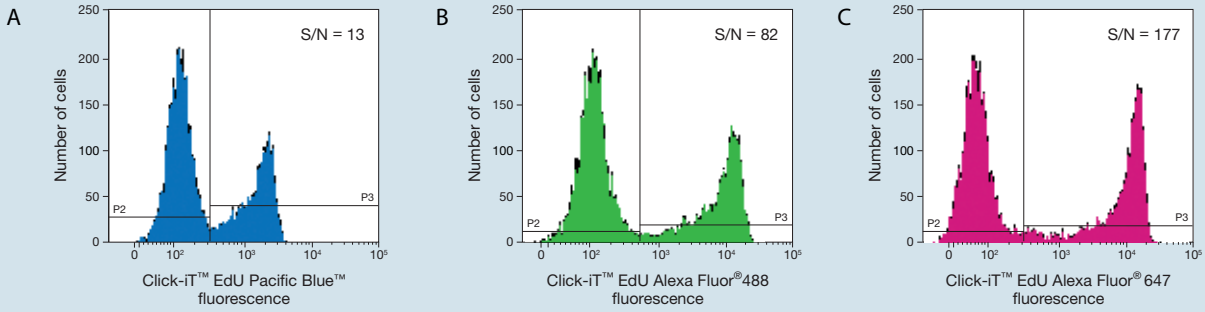

Figure 3—Comparison of the fluorescence signals from the Click-iT™ EdU Pacific Blue™, Alexa Fluor® 488, and Alexa Fluor® 647 Flow Cytometry Assay Kits. Jurkat (human T cell leukemia) cells were treated with 10 µM EdU for 2 hours and detected according to the staining protocol. (A) Cells stained with Pacific Blue™ azide, detected using 405 nm excitation and a 450/50 bandpass filter. (B) Cells stained with Alexa Fluor® azide, detected using 488 nm excitation and a 530/30 bandpass filter. (C) Cells stained with Alexa Fluor® 647 azide, detected using 633 nm excitation and a 660/20 bandpass filter. Signal to noise (S/N) was calculated by dividing the median Click-iT™ EdU positive population (P3) by the median nonproliferating population (P2) indicated by the markers.

Click-iT™ EdU products are available exclusively from Invitrogen

- Click-iT™ EdU for flow cytometry—In addition to the original Alexa Fluor® 488 dye–based Click-iT™ EdU flow cytometry assay, Invitrogen now offers kits that include either the Pacific Blue™ dye or the Alexa Fluor® 647 dye, keeping the valuable 488 nm laser open (Figure 3). The Pacific Blue™ dye is optimal for instruments with a violet or 405 nm laser excitation source, and the Alexa Fluor® 647 dye is optimal for instruments with a red or 633/635 nm laser excitation source. All three flow cytometry kits include sufficient materials to perform 50 assays in a 0.5 ml volume: 10 mg EdU, two cell cycle analysis dyes compatible with the Click-iT™ EdU detection reagent, fixation and permeabilization reagents, and Click-iT™ detection buffer.
- Click-iT™ EdU for fluorescence microscopy—To visualize proliferating cells grown on coverslips, simply follow the recently developed technical tip "Conversion of the Click-iT™ EdU High-Throughput Imaging (HCS) Kit for Conventional Fluorescence Microscopy" shipped with our Click-iT™ EdU 2-plate assays (and available for download from our website), and generate your own stunning multicolor image (Figure 4).
- Click-iT™ EdU for high-throughput imaging (HCS)—Click-iT™ EdU assays are the assays that HCS platforms have been waiting for.

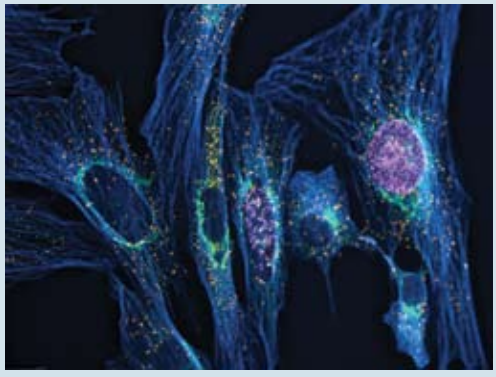

Figure 4—Multicolor imaging is a snap with Click-iT™ EdU. Muntjac cells were treated with 10 µM EdU for 45 minutes. Cells were then fixed and permeabilized, and EdU that had been incorporated into newly synthesized DNA was detected by the far red–fluorescent Click-iT™ EdU Alexa Fluor® 647 High-Throughput Imaging (HCS) Assay (A10208), utilizing the technical tip for converting the HCS assay to conventional fluorescence microscopy (document X10027). Tubulin was labeled with an anti-tubulin antibody and visualized with an Alexa Fluor® 350 goat anti–mouse IgG antibody (A21049). The Golgi complex was stained with the green-fluorescent Alexa Fluor® 488 conjugate of lectin HPA from *Helix pomatia* (edible snail) (L11271), and peroxisomes were labeled with an anti-peroxisome antibody and visualized with an orange-fluorescent Alexa Fluor® 555 donkey anti–rabbit IgG antibody (A31572).

The ease of use and multiplex capability of these kits represent a quantum leap in the HCS analysis of cell proliferation—assays that once had to be run in parallel can now be run in the same well with Click-iT™ EdU (Figure 5). The Click-iT™ EdU High-Throughput Imaging (HCS) assay kits contain one of the stellar Alexa Fluor® dyes—the green-fluorescent Alexa Fluor® 488, the red-fluorescent Alexa Fluor® 594, or the far red–fluorescent Alexa Fluor® 647—and EdU, Click-iT™ detection buffer, and Hoechst 33342 for cell registration or cell cycle analysis.

- Click-iT™ EdU for *in vivo* applications—EdU can be substituted into any existing BrdU application, including *in vivo* applications. Animals can be injected or fed EdU (A10044) at the same concentrations (or potentially even lower) as BrdU for subsequent analysis with one of the Click-iT™ EdU flow cytometry or HCS assay kits.

To EdU-cate yourself further about this innovative new technology, visit **www.invitrogen.com/edu.** ■

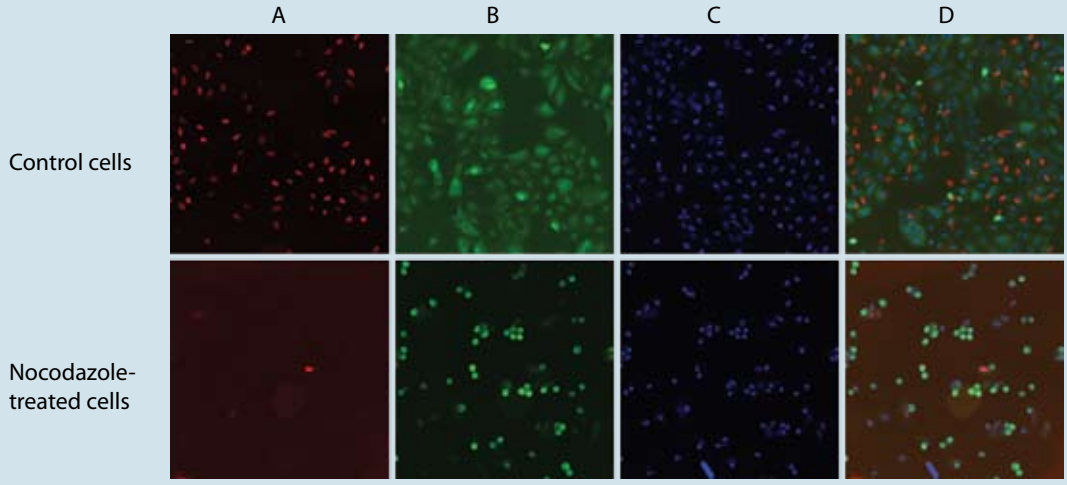

Figure 5—Click-iT™ EdU enables content-rich results on HCS platforms, currently not possible with BrdU. A549 cells were treated with 170 nM nocodazole, a G_2/M block, for 24 hours. Both the treated and control cells were then pulsed with 10 µM EdU for 30 minutes. Cells were fixed and permeabilized, and EdU that had been incorporated into newly synthesized DNA was detected using the red-fluorescent Click-iT™ EdU Alexa Fluor® 594 High-Throughput Imaging (HCS) Assay (A). Cyclin B1 was detected with an anti–cyclin B1 antibody (AHF0062) and visualized with an Alexa Fluor® 488 goat anti–rabbit IgG antibody (A11008) (B). Nuclei were counterstained with the blue-fluorescent Hoechst 33342 (C), which can also be used for cell cycle analysis. The composite image containing all 4 stains is shown in (D). Imaged and analyzed using Thermo-Fisher Cellomics ArrayScan® VTI.

Product	Quantity	Cat. no.
Click-iT™ EdU Alexa Fluor® 488 High-Throughput Imaging (HCS) Assay, 2-plate size	1 kit	A10027
Click-iT™ EdU Alexa Fluor® 488 High-Throughput Imaging (HCS) Assay, 10-plate size	1 kit	A10028
Click-iT™ EdU Alexa Fluor® 594 High-Throughput Imaging (HCS) Assay, 2-plate size	1 kit	A10209
Click-iT™ EdU Alexa Fluor® 647 High-Throughput Imaging (HCS) Assay, 2-plate size	1 kit	A10208
Click-iT™ EdU Alexa Fluor® 647 Flow Cytometry Assay Kit, 50 assays	1 kit	A10202
Click-iT™ EdU Pacific Blue™ Flow Cytometry Assay Kit, 50 assays	1 kit	A10034
Click-iT™ EdU Alexa Fluor® 488 Flow Cytometry Assay Kit, 50 assays	1 kit	C35002
EdU (5-ethynyl-2′-deoxyuridine)	50 mg	A10044

Phospholipase activity detection from A to D

NEW PLA_1- AND PLA_2-SPECIFIC SUBSTRATES.

Fluorogenic phospholipase A substrates

The importance of phospholipases in cellular signaling, lipid metabolism, and inflammatory responses, as well as pathological disorders related to these processes, has stimulated demand for fluorescence-based activity monitoring methods.[1–6] Molecular Probes® fluorogenic phospholipase A substrates are designed to provide continuous monitoring of phospholipase A (PLA) activity in purified enzyme preparations, cell lysates, and living cells. Applications of these substrates extend from clinical assays for serum PLA_2[7] to *in vivo* small animal imaging[8] (Figure 1). The substrates are dye-labeled phospholipids of two types—glycerophosphocholines with BODIPY® dye–labeled *sn*-1 and *sn*-2 acyl or alkyl chains (Figure 2A), and glycerophosphoethanolamines with BODIPY® dye–labeled acyl chains and dinitrophenyl quencher-modified head groups (Figure 2B). These structural variations determine specificity for PLA_1 versus PLA_2 and the fluorescence response associated with enzymatic cleavage of the substrate, as summarized in Table 1.

New Red/Green BODIPY® PC-A2

Red/Green BODIPY® PC-A2 provides a capacity for dual-emission fluorescence ratio detection that is not afforded by other fluorogenic phospholipase A substrates (Figure 3). Cleavage of the BODIPY® FL pentanoic acid substituent at the *sn*-2 position results in decreased quenching by fluorescence resonance energy transfer (FRET) to the BODIPY® 558/568 dye attached to the *sn*-1 position (Figure 2A). The result is a PLA_2-dependent increase in BODIPY® FL dye fluorescence emission detected in the 515–545 nm range. The FRET-sensitized BODIPY® 558/568 dye fluorescence signal is expected to show a reciprocal decrease. In practice, BODIPY® 558/568 dye fluorescence may show either a decrease or a slight increase (Figure 3C), depending on the formulation of the substrate and the instrument excitation/emission wavelength settings. The dual emission properties of this substrate also provide the capacity to localize the lysophospholipid and fatty acid products of PLA_2 cleavage via their distinct spectroscopic signatures in imaging experiments.[8]

New PED-A1 substrate for phospholipase A_1

Despite their key roles in lipid metabolism, class A_1 phospholipases have received much less attention from researchers than A_2 class enzymes. For example, inhibition of lysosomal phospholipase A_1 activity by polycationic antibiotics or amphiphilic cationic drugs is considered to be responsible for the development of drug-induced lysosomal phospholipidosis in cells and tissues.[9] Our new PED-A1 substrate is designed for specific detection of PLA_1 activity. PED-A1 is structurally and mechanistically similar to the PLA_2 substrate PED6, the major difference being that the cleavable BODIPY® FL pentanoic acid substituent is attached at the *sn*-1 position (Figure 2B).

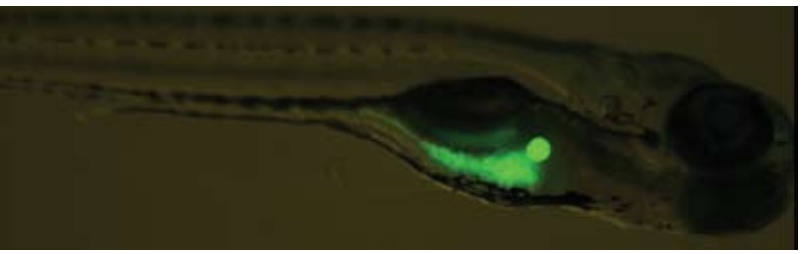

Figure 1—Imaging of lipid digestion pathways in zebrafish (*Danio rerio*) using the fluorogenic phospholipase A_2 substrate PED6. A zebrafish larva (5 days post-fertilization) was incubated with PED6 for 2 hours. Localized fluorescence in the gallbladder and intestinal lumen results from endogenous lipase activity and rapid transport of the substrate cleavage products through the intestinal and hepatobiliary systems. Image contributed by Steven A. Farber, Carnegie Institute of Washington.

Amplex® Red Phospholipase C and D Assay Kits

The Amplex® Red Phosphatidylcholine-Specific Phospholipase C (PC-PLC) and Phospholipase D (PLD) Assay Kits provide fluorometric enzyme-coupled methods for continuous monitoring of the respective enzymes activities. Each kit provides detailed protocols and sufficient reagents for approximately 500 assays using a fluorescence microplate reader and a reaction volume of 200 µl per assay. →

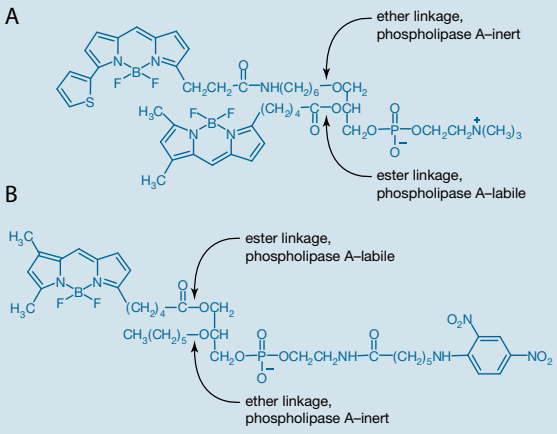

Figure 2—Structures of (**A**) Red/Green BODIPY® PC-A2 and (**B**) PED-A1.

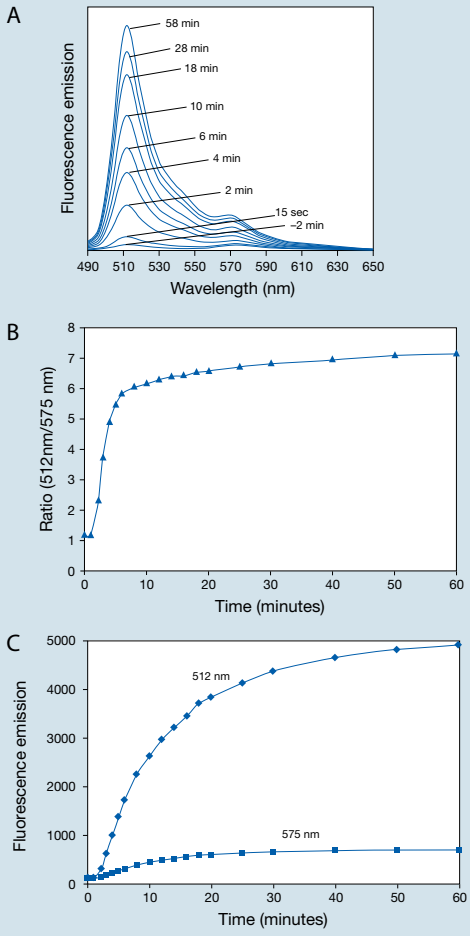

Figure 3—PLA_2 response characteristics of Red/Green BODIPY® PC-A2 substrate. (A) Fluorescence emission spectra (excitation ~480 nm) of Red/Green BODIPY® PC-A2 (5 µM) incorporated in liposomes containing 25 µM DOPC and 25 µM DOPG. In descending order, the topmost seven nested curves represent time points 58, 28, 18, 10, 6, 4, and 2 minutes after addition of 0.5 units of bovine pancreatic PLA_2. The two curves closest to the x-axis baseline represent 15 seconds after enzyme addition and 2 minutes before addition. (B) Plot of the ratio of green (512 nm) to red (575 nm) fluorescence emission intensities vs. time, derived from data shown in (A). PLA_2 addition at t = 2 minutes. (C) Plot of green (512 nm) and red (575 nm) fluorescence emission intensities vs. time, derived from data shown in (A). PLA_2 addition at t = 2 minutes.

Table 1—Fluorogenic phospholipase A substrates.

Substrate	Specificity	Cleavage product *	Detection †	Cat. no.
bis-BODIPY® FL C_{11}-PC	PLA_1 or PLA_2	D3862	Fluorescence intensity increase, Ex = 488 nm, Em = 530 nm	B7701
Red/Green BODIPY® PC-A2	PLA_2	D3834	Fluorescence emission ratio increase, Ex = 488 nm, Em = 530/590 nm ‡	A10072
PED6	PLA_2 §	D3834	Fluorescence intensity increase, Ex = 488 nm, Em = 530 nm	D23739
PED-A1	PLA_1	D3834	Fluorescence intensity increase, Ex = 488 nm, Em = 530 nm	A10070

* Catalog number of the fatty acid product generated by action of the enzyme. These materials are useful as standards for evaluating percentage substrate conversion in enzymatic reactions. † Fluorescence signal corresponding to increasing phospholipase A activity. Ex = excitation wavelength; Em = emission wavelength. Instrument settings need to be closely but not exactly matched to these wavelength specifications. ‡ May also be monitored via fluorescence intensity increase, Ex = 488 nm, Em 530 nm, if ratiometric readout is not desired. § PED6 may be cleaved by PLA_1, but this reaction does not result in separation of the fluorophore and quencher substituents.

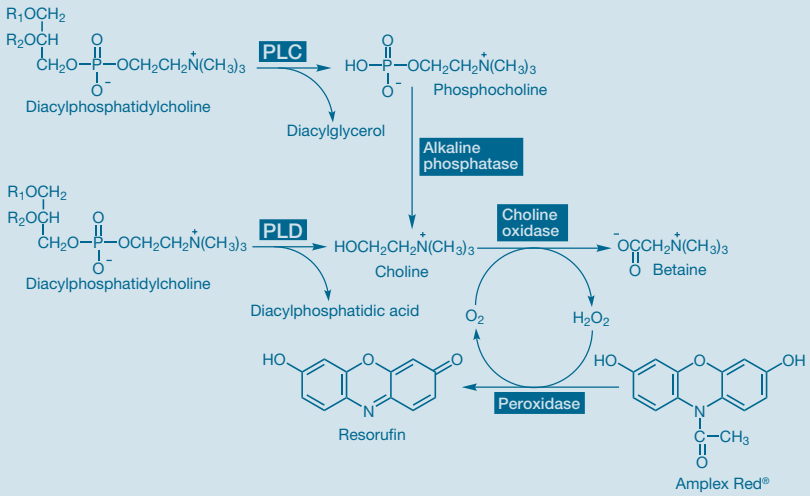

Figure 4—Detection scheme utilized in the Amplex® Red Phospholipase D (PLD) and Phosphatidylcholine-Specific Phospholipase C (PLC) assays. Diacylphosphatidylcholine substrates (R_1 and R_2 represent fatty acyl substituents) are converted in one or two enzyme-catalyzed steps to choline. Subsequent oxidation of choline is quantitatively coupled via H_2O_2 to generation of fluorescent resorufin from the Amplex® Red reagent, mediated by horseradish peroxidase (HRP).

Both assays are based on oxidation of choline by choline oxidase generating H_2O_2, which is then used as a substrate for horseradish peroxidase–mediated oxidation of the nonfluorescent Amplex® Red reagent to fluorescent resorufin (excitation/emission maxima ~571/585 nm) (Figure 4). PLD quantitation data from *Streptomyces chromofuscus* are shown in Figure 5. The PC-PLC assay involves an additional coupling step in which phosphocholine is converted to choline by the action of alkaline phosphatase. Balcerzak and coworkers have recently proposed some modifications to these assays to improve discrimination between PC-PLD and PLD activities.[10] Other recent applications of these assays include characterizing the involvement of PC-PLC and PLD in interleukin 1β (IL-1β) secretion[11] and B lymphocyte activation[12] pathways. ■

References

1. Schaloske, R.H. and Dennis, E.A. (2006) *Biochim Biophys Acta* 1761:1246–1399.
2. Scott, K.F. et al. (2003) *Expert Opin Ther Targets* 7:427–440.
3. Kalyvas, A. and David, S. (2004) *Neuron* 41:323–335.
4. Sved, P. et al. (2004) *Cancer Res* 64:6934–6940.
5. Law, M.H. et al. (2006) *Mol Psychiatry* 11:547–556.
6. White, M.C. and McHowat, J. (2007) *Cardiovasc Hematol Agents Med Chem* 5:91–95.
7. Tsao, F.H. (2007) *Clin Chim Acta* 379:119–126.
8. Farber, S.A. et al. (2001) *Science* 292:1385–1388.
9. Piret, J. et al. (2005) *Chem Phys Lipids* 133:1–15.
10. Balcerzak, M. et al. (2006) *FEBS Lett* 580:5676–5680.
11. Andrei, C. et al. (2004) *Proc Natl Acad Sci U S A* 101:9745–9750.
12. Moreno-García, M.E. et al. (2005) *J Immunol* 174:2687–2695.

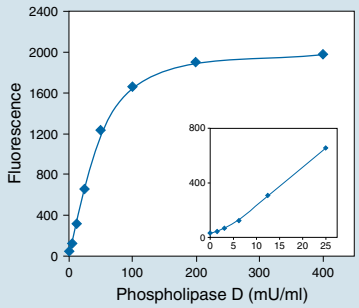

Figure 5—Quantitation of phospholipase D from *Streptomyces chromofuscus* using the Amplex® Red Phospholipase D Assay Kit (A12219). Fluorescence was measured with a fluorescence microplate reader using excitation at 530 ± 12.5 nm and fluorescence detection at 590 ± 17.5 nm. The inset shows the sensitivity at very low enzyme concentrations (0–25 mU/ml).

Product	Quantity	Cat. no.
Red/Green BODIPY® PC-A2 (1-O-(6-BODIPY® 558/568-aminohexyl)-2-BODIPY® FL C5-*sn*-glycero-3-phosphocholine), ratiometric phospholipase A_2 substrate	100 µg	A10072
PED-A1 (N-((6-(2,4-DNP)amino) hexanoyl)-1-(BODIPY® FL C5)-2-hexyl-*sn*-glycero- 3-phosphoethanolamine), phospholipase A_1 selective substrate	100 µg	A10070
Amplex® Red Phosphatidylcholine-Specific Phospholipase C Assay Kit, 500 assays	1 kit	A12218
Amplex® Red Phospholipase D Assay Kit, 500 assays	1 kit	A12219
Amplex® Red/UltraRed stop reagent, 500 tests	1 set	A33855

Quantum dots as replacements for tandem dyes in flow cytometry

EFFICIENT EXCITATION USING VIOLET AND UV LASERS.

In flow cytometry, investigators achieve greater multiplexing of cellular markers using tandem dyes—long wavelength–emitting organic dyes coupled to the fluorescent proteins R-phycoerythrin (RPE) or allophycocyanin (APC). Although these RPE and APC tandem dyes provide far-red emission using 488 and 633 nm laser excitation, respectively, they suffer from poor stability, batch variability, and spectral bleed-through of donor dyes. Qdot® nanocrystals—nanometer-scale (roughly protein-sized) semiconductor atom clusters—are extremely efficient materials for generating fluorescence, and provide fluorescent labels that can be excited with UV or violet light sources as well as with longer-wavelength light sources, and exhibit long, effective Stokes shifts and relatively narrow emission peaks. Qdot® nanocrystals can add two to five colors to the antibody palette and have proven useful in a number of flow cytometry applications, including an 18-color panel for immunophenotyping multiple antigen-specific T cell populations.[1]

Here, we focus on the two longest wavelength–emitting Qdot® nanocrystals currently available—Qdot® 705 and Qdot® 800 nanocrystals. Using fluorescent streptavidin conjugates to detect surface CD4 antigen on live human peripheral blood leukocytes, we compare the performance of these fluorophores to that achieved with RPE or APC tandem dyes, which also emit in the far-red spectral region. Even with suboptimal excitation at 488 and 633 nm, Qdot® 705 and Qdot® 800 conjugates provided better resolution of CD4-positive and CD4-negative populations than did RPE and APC tandem dyes in the far-red emission regions. Furthermore, in contrast to tandem dyes, Qdot® nanocrystals do not exhibit any fluorescence emission in the RPE or APC emission regions and are efficiently excited by all common lasers (Figure 1) used in flow cytometers.

Human peripheral blood leukocytes were stained with biotin–anti-CD4 (Invitrogen) and fluorescent streptavidin conjugates using standard protocols for indirect staining.[2] Stained samples were analyzed on a BD™ LSR II flow cytometer (BD Biosciences) equipped with 405 nm, 488 nm, 532 nm, and 633 nm lasers. Table 1 shows the emission filters used for analyses. Signal-to-background ratios (S/B) were calculated as positive-peak median fluorescence divided by negative-peak median fluorescence. →

Table 1—Primary excitation wavelengths and emission filters used for the fluorophores in this study.

Fluorophore	Excitation (nm)	Emission filter *
Qdot® 705 nanocrystal	405	710 ± 10
Qdot® 800 nanocrystal	405	780 ± 30
RPE	488	585 ± 21
RPE–Alexa Fluor® 680 tandem	488	695 ± 20
RPE-Cy®5.5 tandem	488	695 ± 20
RPE-Cy®7 tandem	488	780 ± 30
APC	633	660 ± 10
APC-Cy®5.5 tandem	488	695 ± 20
APC–Alexa Fluor® 700 tandem	633	710 ± 10
APC-Cy®7 tandem	633	780 ± 30

* Mean wavelength ± half peak bandwidth.

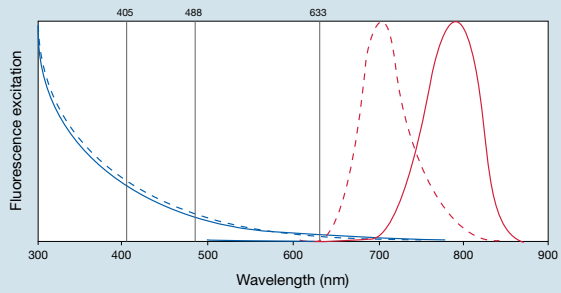

Figure 1—Excitation (blue) and emission (red) spectra of two long wavelength–emitting Qdot® nanocrystals. The exitation and emission spectra are shown for Qdot® 705 (dashed) and Qdot® 800 (solid) nanocrystals. These Qdot® nanocrystals can be substituted for tandem dyes containing Cy®5.5, and Cy®7, respectively. Common laser lines are also shown as vertical lines at 405, 488, and 633 nm.

Broad excitation spectra and narrow emission spectra of Qdot® nanocrystals

Qdot® nanocrystals can be excited with a wide range of wavelengths; excitation efficiency decreases with increasing wavelength. Strong excitation is obtained with UV or violet lasers (405–407 nm), but the nanocrystals can be efficiently excited with other common lasers on flow cytometers that provide 488 nm, 532 nm, and 633 nm excitation. In contrast to their broad excitation spectra, Qdot® nanocrystals have relatively narrow and symmetrical emission profiles.

Cross-laser excitation of Qdot® nanocrystals

Figure 2 compares CD4-positive and CD4-negative populations of cells stained with Qdot® 705, RPE-Cy®5.5 tandem, and RPE–Alexa Fluor® 680 tandem conjugates and excited by 405 nm, 488 nm, and 633 nm laser light. Qdot® 705 conjugate–labeled cells showed strong separation of CD4-positive and CD4-negative populations when excited with 405 nm light, as well as when excited with 488 nm and 633 nm light. The RPE–Alexa Fluor® 680 tandem conjugate showed better resolution with 488 nm excitation than did the RPE-Cy®5.5 tandem conjugate, but the Qdot® 705 conjugate with 488 nm excitation provided at least twice the population separation (S/B = 78.9). Both tandem dyes showed direct excitation of their acceptor dyes with 633 nm excitation, as well as weaker excitation of the RPE with 405 nm light. Thus, these tandem dyes demonstrate spectral overlap that must be corrected for in multicolor experiments.

Under the same experimental conditions, cells stained with Qdot® 705 conjugates exhibited S/B ratios more than 10 times higher than those of cells stained with APC–Alexa Fluor® 700 and APC-Cy®5.5 tandem conjugates using 633 nm excitation (Figure 3). APC was also found to be weakly excited by 405 nm light (data not shown).

Spectral overlap of Qdot® nanocrystals versus tandem dyes

Figure 4 shows the effect of spectral overlap on data analysis using Qdot® 800 nanocrystals and RPE-Cy®7 tandem dye with uncompensated

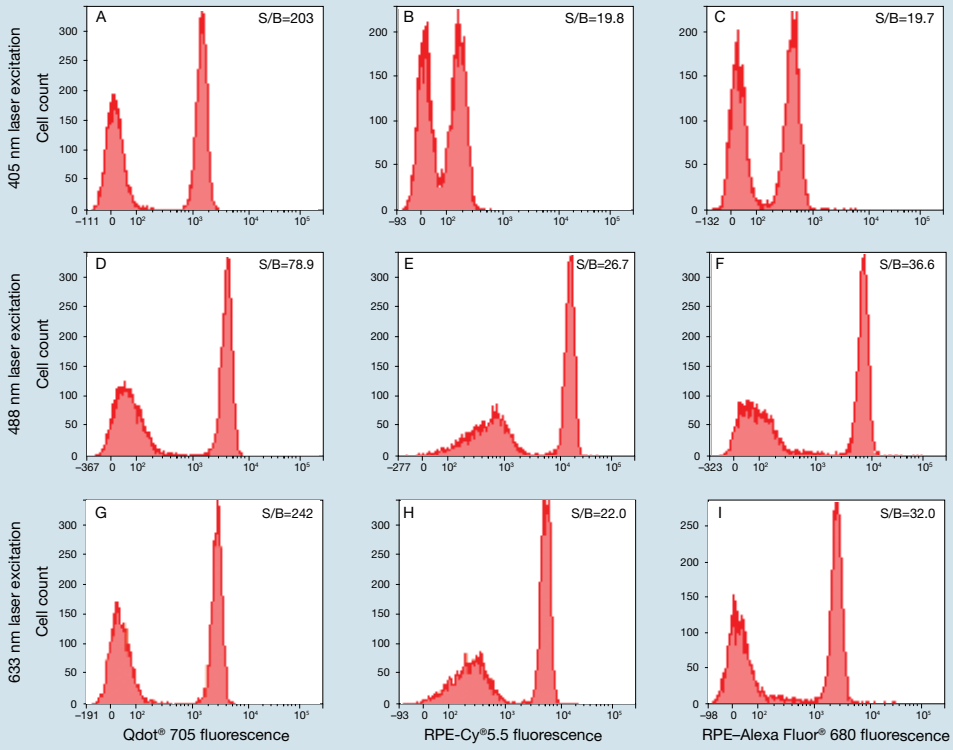

Figure 2—Comparison of Qdot® 705, RPE-Cy®5.5, and RPE-Alexa Fluor® 680 conjugates excited at three different wavelengths. Human mononuclear cells were stained with biotin anti–human CD4 antibody, followed by a streptavidin conjugate of Qdot® 705 nanocrystals (A, D, G), RPE-Cy®5.5 tandem dye (B, E, H), or RPE–Alexa Fluor® 680 tandem dye (C, F, I). S/B = signal-to-background ratio.

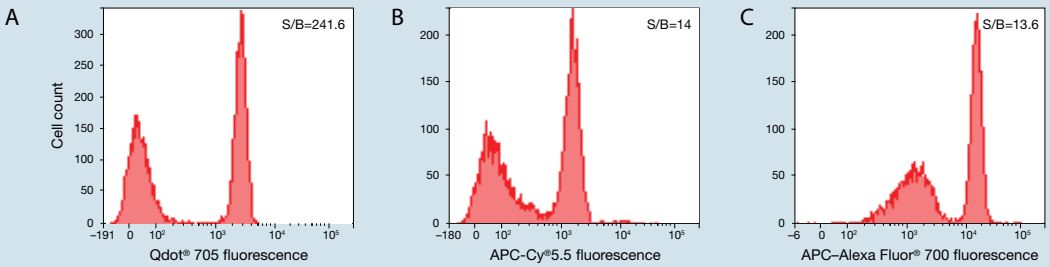

Figure 3—Comparison of Qdot® 705, APC-Cy®5.5, and APC–Alexa Fluor® 700 conjugates excited at 633 nm. Human mononuclear cells were stained with biotin anti–human CD4 antibody, followed by a streptavidin conjugate of Qdot® 705 nanocrystals (A), APC-Cy®5.5 (B), or APC–Alexa Fluor® 700 tandem dye (C).

data. With the RPE-Cy®7 tandem conjugate, the CD4-positive population is bright in the RPE-Cy®7 channel, but also shows considerable RPE fluorescence as a vertical displacement (Figure 4A). The Qdot® 800 conjugate staining shows a similarly bright CD4-positive population with 405 nm excitation, but no bleedthrough into the RPE channel (Figure 4B). Instead, there is emission in the RPE-Cy®7 channel (Figure 4C), as this channel captures the 780 nm wavelength range off the 488 nm laser. Both overlaps can be removed by compensation, but the tandem dye signal must be removed from the valuable RPE channel (a channel used in nearly every staining experiment) and other channels that capture RPE emission. The Qdot® 800 nanocrystal signal must only be removed from channels that capture the 780 nm range of light. Of course, this correction is only required if the researcher is using a fluor that is detected in that wavelength range.

Qdot® nanocrystals are efficient fluorescent labels when excited with UV or violet light, allowing better resolution of even poorly expressed antigens. Qdot® nanocrystals also provide bright fluorescence, even when excited suboptimally with longer wavelengths, and can provide equivalent or better population resolution than seen with RPE or APC tandem dyes. When nanocrystals are used in combination with conventional dyes, the operator will have to apply laser compensation to remove the nanocrystal signal from fluorophores that are detected in the same wavelength range. Researchers also have the option of using Qdot® nanocrystals with blue to red excitation in place of tandem dyes, particularly on flow cytometers that lack violet excitation. While tandem dyes are widely used for surface and intracellular targets, Qdot® nanocrystal reagents can be particularly useful for surface markers, where researchers are trying to protect the resolution in the RPE or APC channel, or where additional resolution or photostability are useful, as with fluorescence-activated cell sorting.

To select the right Qdot® nanocrystal conjugate for your experiment, see the new Qdot® primary antibody conjugates, and place your order, visit us at **www.invitrogen.com/qdotinflow**. ■

References

1. Chattopadhyay, P.K. et al. (2006) *Nat Med* 12:972–977.
2. Stewart, C.C. and Stewart, S.J. (1997) Immunophenotyping, In *Current Protocols in Cytometry* (Robinson, J. P., ed., John Wiley and Sons, New York). 6.2.1–6.2.18.

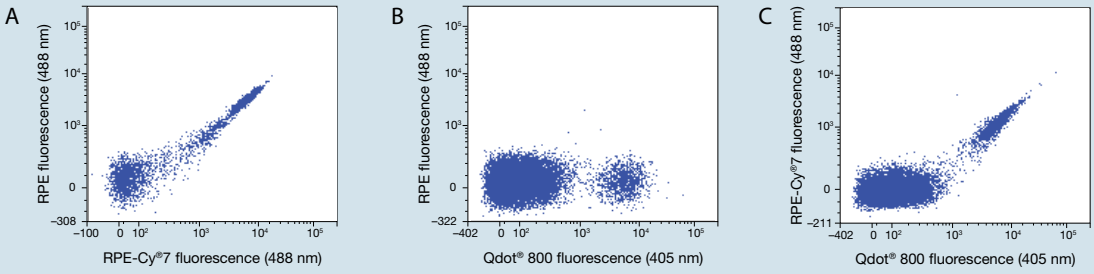

Figure 4—Comparison of RPE-Cy®7 and Qdot® 800 conjugates. Human mononuclear cells were stained with biotin anti–human CD4 antibody, and streptavidin conjugates of RPE-Cy®7 tandem dye (A) or Qdot® 800 nanocrystals (B, C). For each conjugate dot plot, the x-axis shows emission in the primary fluorescence channel and the y-axis shows emission in potential overlap channels. The excitation wavelength is in parentheses. Data are shown without compensation for spectral overlap.

Mitochondria and cardiac disorders

ANTIBODIES AGAINST PROTEINS IN THE OXIDATIVE PHOSPHORYLATION SYSTEM.

Invitrogen offers a broad range of antibodies against key components of the mitochondrial oxidative phosphorylation (OxPhos) system that are validated for imaging (Figure 1) and western blot applications. The authors of the publication highlighted in this feature were able, in part, to show the relationship between mitochondrial impairment and cardiac failure through the use of several of these validated antibodies.

Mitochondrial function is traditionally associated with the production of energy in the form of ATP. More recently, reseach on mitochondrial physiology has greatly expanded to encompass such diverse cellular roles as amino acid metabolism, lipid oxidation, heat production, calcium ion buffering, and apoptosis. With such broad biological roles, it is not surprising that aberrancies in mitochondrial function have been linked to human disease. Recently, mitochondrial function has been linked more closely to cardiac disorders.

A recent paper by Nojiri and coworkers[1] shows that accumulated oxidative stress impairs mitochondrial respiration, and that superoxide generated in mitochondria may play a pivotal role in the development and progression of heart failure. Here the authors were able to generate a heart- and muscle-specific manganese superoxide dismutase (Mn-SOD) mouse knockout model, termed H/M-*Sod2*$^{-/-}$, using the Cre-loxP system under the control of the muscle creatine kinase promoter. These mice showed progressive congestive heart failure attributed to cardiac muscle degeneration, quite different from the phenotypes observed with total *Sod2*$^{-/-}$ deficient animals that display highly complex pathologies. With this new model of cardiac failure, the authors were able to demonstrate that deficiencies in Mn-SOD globally reduced mitochondrial respiration (Figure 2). Using a combination of blotting and imaging methods, the authors showed that H/M-*Sod2*$^{-/-}$ animals were highly defective in Complex II activity, and protein expression of Complexes I, II, III, and V was greatly reduced. Curiously, mRNA levels of these proteins remained unchanged, suggesting that reactive oxygen species (ROS) may reduce mitochondrial OxPhos activity at the protein level rather than through previously described redox-sensitive transcriptional effectors such as NFκB and AP-1.[2,3]

Table 1 shows the antibodies used by Nojiri and coworkers and are just a few of the anti-OxPhos antibodies Invitrogen offers. To see the complete product line, visit **www.invitrogen.com**. ■

References

1. Nojiri, H. et al. (2006) *J Biol Chem* 281:33789–33801.
2. Bowie, A. and O'Neill, L.A. (2000) *Biochem Pharmacol* 59:13–23.
3. Wu, S. et al. (2005) *Free Radic Biol Med* 39:1601–1610.

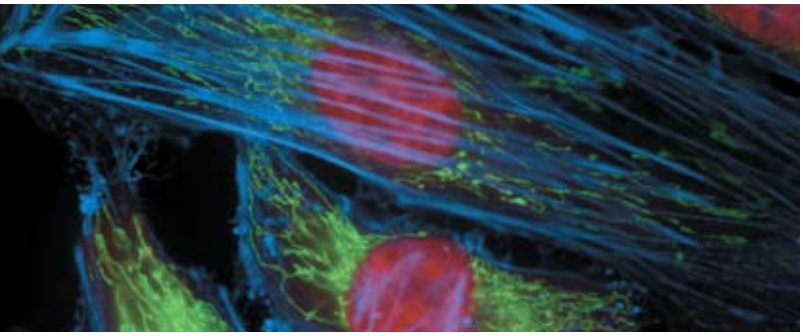

Figure 1—Fixed and permeabilized HeLa cells stained with Alexa Fluor® 350 phalloidin, an anti–OxPhos Complex V inhibitor protein antibody, and anti–cdc6 peptide antibody. The anti–OxPhos Complex V inhibitor protein antibody was prelabeled with the Zenon® Alexa Fluor® 488 Mouse IgG1 Labeling Kit, and the anti–cdc6 peptide antibody was prelabeled with the Zenon® Alexa Fluor® 568 Mouse IgG1 Labeling Kit.

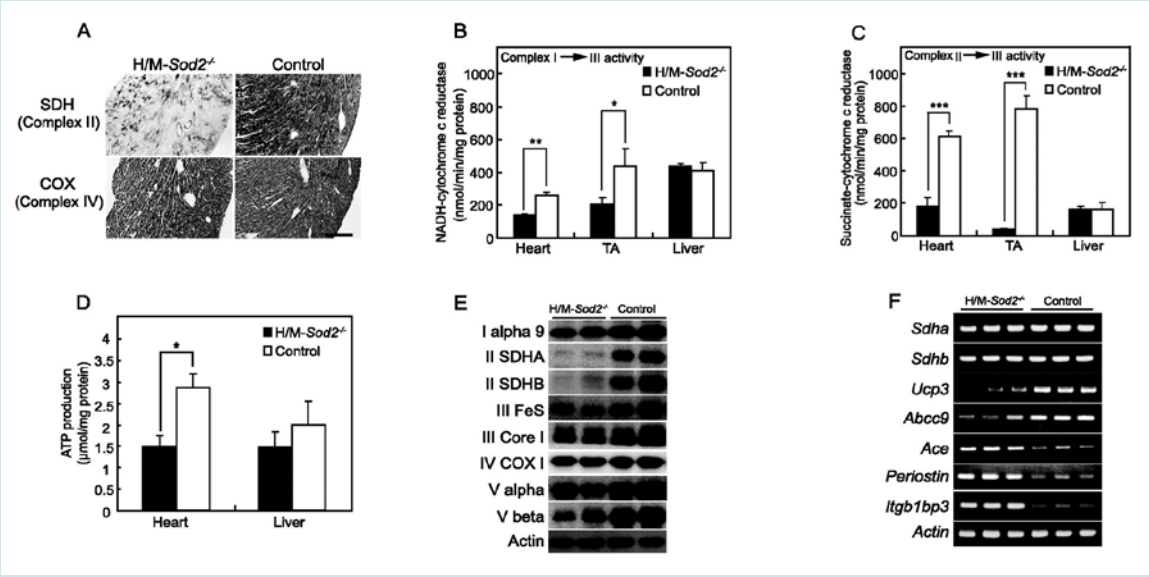

Figure 2—Impaired mitochondrial respiratory activities. (A) enzymatic histochemical staining for SDH (top) and COX activities (bottom) in hearts from 15-week-old mice of the indicated genotypes (scale bar = 50 µm). (B) and (C) OxPhos enzyme activities of heart, TA muscle, and liver mitochondria in H/M-*Sod2*$^{-/-}$ mice (n = 3) or control mice (n = 3) at 15 weeks of age. Activities of OxPhos Complex I + III (B) and Complex II + III (C) are shown (*, $p < 0.05$; **, $p < 0.005$; ***, $p < 0.0005$). (D) production of ATP in heart and liver mitochondria. ATP production in heart mitochondria from H/M-*Sod2*$^{-/-}$ mice (n = 5) was lower than that from control mice (n = 4; *, $p < 0.05$). In liver mitochondria, ATP production was not significantly different between H/M-*Sod2*$^{-/-}$ (n = 3) and control (n = 3) mice. Results are represented by mean ± SE. (E) Western blot analysis of proteins extracted from heart of 15-week-old H/M-*Sod2*$^{-/-}$ mice using antibodies against OxPhos subunits and actin. (F) transcriptional alterations of Sdha, Sdhb, Ucp3, Abcc9, Ace, periostin, Itgb1bp3, and actin genes in hearts (n = 3). Figure reproduced from *J Biol Chem* (2006) 281:33796 with permission from the American Society for Biochemistry and Molecular Biology.

Table 1—Mitochondrial OxPhos antibodies.

Complex	Name		Molecular weight *	Alternative name	Protein number †	Gene number ‡	Clone/Isotype	Reactive species §	Cat. no. **
I	NADH–ubiquinone oxidoreductase	39,000 Da subunit	42.5	α-subcomplex, 9	Q16795	NDUFA9	20C11 (Ms IgG1κ)	B, H, Ms, Rt	A21344
II	Succinate–ubiquinone oxidoreductase	70,000 Da subunit	72.7	Flavoprotein	P31040	SDHA	2E3 (Ms IgG1κ)	B, H, Ms, Rt	A11142
		30,000 Da subunit	31.6	Iron–sulfur protein	P21912	SDHB	21A11 (Ms IgG2aκ)	B, H, Ms, Rt	A21345
III	Ubiquinone–cytochrome *c* oxidoreductase	Core 1 subunit	51.6	None	P31930	UQCRC1	16D10 (Ms IgG1κ)	B, H, Ms	A21362
		Iron–sulfur subunit	29.6	Rieske iron–sulfur protein	P47985	UQCRFS1	5A5 (Ms IgG2bκ)	B, H, Ms	A21346
IV	Cytochrome *c* oxidase (COX)	Subunit I	57.0	COX I	P00395	MTCO1	1D6 (Ms IgG2aκ)	B, H, Ms, Rt	A6403
V	ATP synthase	β-subunit	56.6	F1 complex, β-subunit	P06576	ATP5B	3D5 (Ms IgG1κ)	B, H, Ms	A21351

*Molecular weight in kilodaltons. † Protein reference numbers are from the Swiss-Prot™ database, an annotated protein sequence database (www.ebi.ac.uk/swissprot), and refer to the human sequence unless otherwise noted. ‡ Gene reference numbers are from the GenBank® database, which can be accessed through Entrez (www3.ncbi.nlm.nih.gov/Entrez). § B = bovine; H = human; Ms = mouse; Rt = rat. ** For all the antibodies listed in this table, the unit size is 100 µg, except for A11142 (50 µg).

Identifying Alzheimer's disease biomarkers from human brain tissue

ANTIBODY BEAD-BASED ASSAYS FOR THE LUMINEX® XMAP® PLATFORM.

Tau and its hyperphosphorylated forms along with β amyloid peptide (Aβ) and its cleavage variants comprise the major constituents of intracellular neurofibrillary tangles and extracellular senile plaques, two hallmarks of Alzheimer's disease brains. Determining the content of total tau, phosphorylated tau, and the cleavage variants of β amyloid in tissues can provide useful information about factors that influence the rate of production and/or accumulation of these analytes.

Our multiplexable immunoassays were developed specifically for detecting and quantitating Alzheimer's disease biomarkers using the Luminex® xMAP® instrument platform. Analytes include Aβ40, Aβ42, total tau, and tau [pT181]. These immunoassays have been thoroughly validated for use with CSF and tissue culture supernatant samples. These assays are also suitable for use in the analysis of brain tissue. In this article we present a detailed procedure for the preparation of brain tissue, and results from the subsequent quantitation of the analytes.

Luminex® immunoassays effectively quantitate AD biomarkers

To demonstrate the utility of the extraction protocol, brain tissue samples from diseased patients and from age-matched controls were evaluated using the Invitrogen Luminex® neuroscience assays (Figure 1). Aβ40 and total tau were quantitated in a two-plex assay (Cat. no. LHB3481, LHB0041, with reagents provided in buffer kit LNB0001), as indicated in the kit protocol. Aβ42 and tau [pT181] were quantitated in a second two-plex assay (Cat. no. LHB3441, LHB7051, with reagents provided in buffer kit LNB0001). Based on the data generated from the preliminary studies, the sample was diluted 1:200 prior to running multiplex assays. The results demonstrate that the sensitivity of these immunoassays is sufficient to permit quantitation of biomarker levels in brain tissue homogenates from disease samples and age-matched controls.

Based on the data presented here, the Invitrogen antibody bead assays for the Luminex® platform are well suited for the detection and quantitation of Alzheimer's disease biomarkers in extracted brain

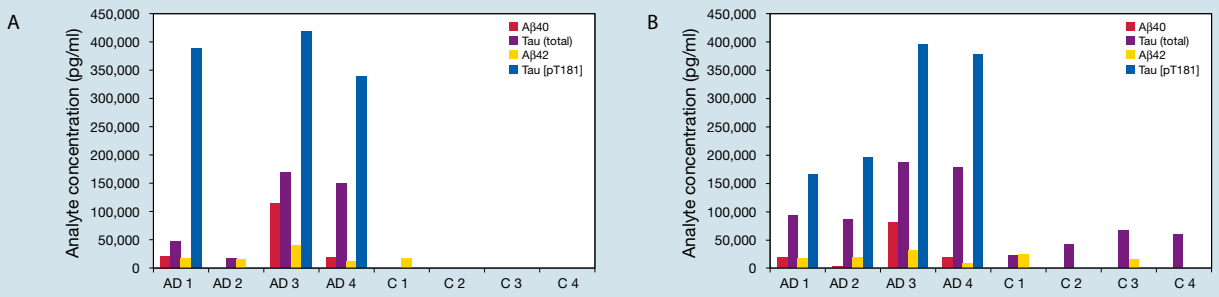

Figure 1—Solubilities of Aβ40, Aβ42, total tau, and tau [pT181] from Alzheimer's disease brains and age-matched control brains. The data show that both of the commonly used detergents Sarkosyl (A) and Triton® X-100 (B) are suitable for the extraction of Alzheimer's disease biomarkers from brain tissue. AD = Alzheimer's disease brain tissue, C = control brain tissue.

PROTOCOL

Preparation and extraction of brain tissue homogenate

1. Dissect temporal cortex free of white matter, and determine the exact wet mass in a microcentrifuge tube. Add 10 times the mass in buffer (1 mM Tris, 1 mM EGTA, 1 mM DTT, 10% sucrose, pH 7.5) (i.e., 10 ml of buffer per gram of tissue) to the tube in 50–100 µl aliquots, and grind thoroughly with a handheld motor grinder after each addition.
2. After homogenization, centrifuge at 26,000 × g for 15 min at 4°C to clarify the homogenate.
3. Carefully remove the supernatant and resuspend the pellet with 1% Triton® X-100 or 1% N-lauroylsarcosine (Sarkosyl) in 1 mM Tris, 1 mM EGTA, 1 mM DTT, 10% sucrose, pH 7.5.
4. Centrifuge at 386,000 × g for 20 min at 4°C.
5. Carefully remove the supernatant and wash the pellet twice with water, then once with 70% formic acid.
6. Dry the sample.
7. Dissolve the residue in 5 M guanidine and mix the sample at room temperature for 3–4 hr on an orbital shaker. The sample is stable and can be freeze-thawed many times at this stage.
8. Prepare tissue homogenate assay buffer using the following formulation:
   - 0.2 g/L KCl
   - 0.2 g/L KH_2PO_4
   - 8.0 g/L NaCl
   - 1.150 g/L Na_2HPO_4
   - 5% BSA (Fraction V, low heavy metal, Calbiochem Cat. no. 12659)
   - 0.03% Tween® 20
   - 1x Protease Inhibitor Cocktail (Calbiochem Cat. no. 539131)
   - Bring total volume to 1 L with ultrapure water and adjust pH to 7
9. Dilute the sample with cold tissue homogenate assay buffer at least 1:25, to reduce the guanidine concentration to <200 mM. Clarify the sample by centrifuging at 16,000 × g for 20 min at 4°C.
10. Carefully decant the supernatant and store on ice until use with the Aβ40 (Cat. no. LHB3481), Aβ42 (Cat. no. LHB3441), tau (total) (Cat. no. LHB0041), and tau [pT181] (Cat. no. LHB7051) Invitrogen Luminex® neuroscience assays to quantitate biomarkers. Perform the assays according to the protocol provided in the Neurobiology Buffer Kit (Cat. no. LNB0001).

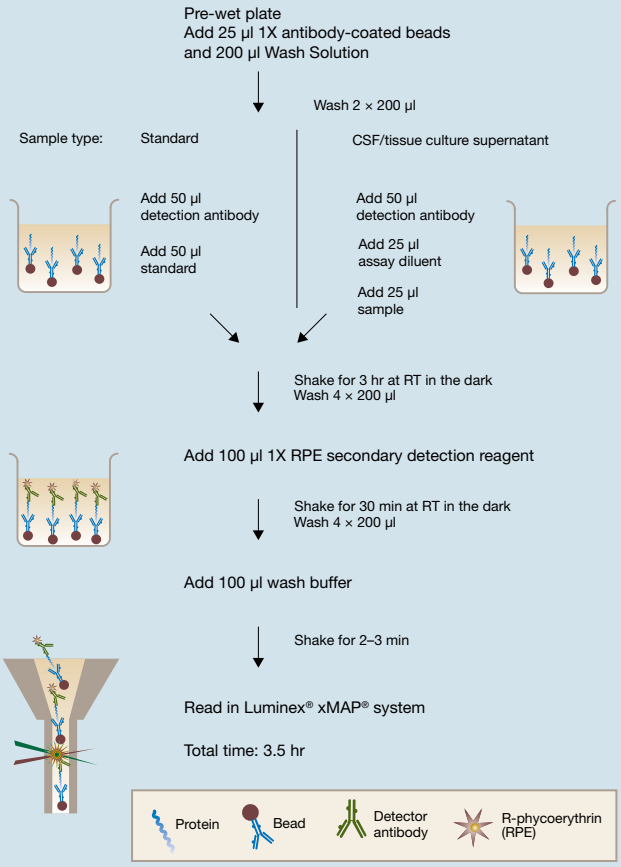

tissue. Changing the buffer from the Assay Diluent provided in the Neurobiology Buffer Kit (which is optimized for CSF and tissue culture medium applications) to the tissue homogenate assay buffer formulation presented (see Protocol, above) improves the performance of the assays with tissue homogenates. A 1:200 dilution for human brain is recommended prior to performing the assay. We recommend that the guanidine concentration for extraction be <200 mM, to achieve linear standard curves and optimal recovery (data not shown).

To learn more about these products, visit **www.invitrogen.com/luminex.** ■

Product	Cat. no.
α-Synuclein Aggregate Antibody Bead Kit (human)	LHB0071
Aβ40 Antibody Bead Kit (human)	LHB3481
Aβ42 Antibody Bead Kit (human)	LHB3441
Aβ Aggregated Antibody Bead Kit (human)	LHB3491
BDNF Antibody Bead Kit (human)	LHC7071
GDNF Antibody Bead Kit (human)	LHC7041
PDGF-BB Antibody Bead Kit (human)	LHG0041
Tau [pS199] Antibody Bead Kit (human)	LHB7041
Tau [pT181] Antibody Bead Kit (human)	LHB7051
Tau [total] Antibody Bead Kit (human)	LHB0041
Neurobiology Buffer Kit	LNB0001

For the type of assay described in this article, you will need an Antibody Bead Kit for each of the analytes you are detecting, the Neurobiology Buffer Kit, and the Luminex® xMAP® instrument.

Measuring proteins in JAK-STAT signaling

QUANTITATE SITE-SPECIFIC PROTEIN PHOSPHORYLATION USING PHOSPHOELISA™ ASSAYS.

The JAK-STAT signaling pathway plays an important role in regulating cell proliferation, differentiation, and apoptosis,[1,2] making identification of inhibitors of the JAK-STAT protein family a focus in oncology and immune suppression research. The phosphorylation status of the proteins involved in the JAK-STAT pathway largely determines the direction of downstream activity. Now you can accurately quantitate phosphorylated protein levels in minimal sample amounts using BioSource™ phosphoELISA™ Kits. These easy-to-perform assays provide highly specific results in as little as four hours.

Following phosphorylation in the JAK-STAT pathway

Upon binding of a variety of cytokines and growth factors to the appropriate receptor, JAK kinases are recruited and activated. JAKs then phosphorylate the receptor's cytoplasmic domain, causing recruitment of STATs, which are in turn phosphorylated, dimerized, and translocated into the nucleus. Once in the nucleus, STAT family members (STAT1, 2, 3, 4, 5a, 5b, and 6) control transcription of specific genes in response to stimulation. Although this basic mechanism of the JAK-STAT pathway is known, very little is known about the details of the recruitment of particular JAK or STAT proteins. For example, cytokine receptors demonstrate preferential use of either a single JAK or a JAK combination, as shown by genetic studies. STATs, on the other hand, have been shown to exhibit either cell type–specific induction of transcription or stereotypic transcription, regardless of cell type. Further studies are required to examine and clarify these restrictions. Since phosphorylation appears to contribute to the activity of these proteins, measuring these levels using the BioSource™ phosphoELISA™ Kits will hopefully help uncover some answers.

Measuring specific phosphorylation

BioSource™ phosphoELISA™ Kits from Invitrogen are now available to specifically measure total and site-specific STAT protein phosphorylation. These simple, unbiased assays enable you to determine STAT protein levels with high specificity and sensitivity in only

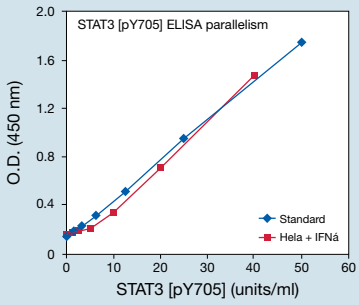

Figure 1—phosphoELISA™ Kit standards parallel natural samples. Recombinant standards are tested against cell lysates to ensure correct measurement values of natural samples. Note that the standard is parallel to the natural sample used.

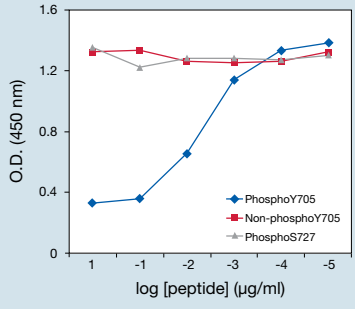

Figure 2—High specificity of the phosphoELISA™ Kit—peptide competition. Peptide blocking is performed on each kit to confirm specificity of the phosphorylation site. The phosphorylated tyrosine 705 blocked the ELISA signal, but not the nonphosphorylated peptide sequence or another phosphopeptide.

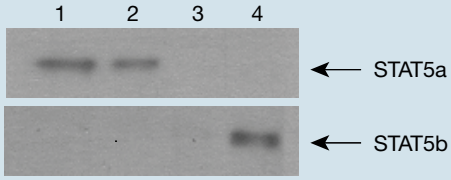

Figure 3—High specificity of the phosphoELISA™ Kit—no cross-reactivity. HEL cell lysates were incubated with the capture antibody used in the STAT5a [pY694] ELISA (lane 2). An antibody specific for STAT5a and STAT5b was used as a positive control (lanes 1 and 4). IgG beads were used as a negative control (lane 3). The capture antibody recognizes the a isoform of STAT5 but not the b isoform. Thus, the STAT5a [pY694] ELISA does not cross-react with the STAT5b protein.

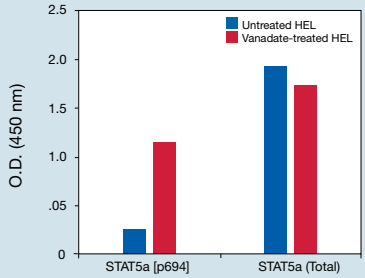

Figure 4—Ensure correct activation patterns. Cell extracts were prepared and analyzed with the STAT5a [pY694] ELISA and STAT5a (Total) ELISA kits. Phosphorylation of STAT5a is increased in sodium vanadate–treated HEL cells, whereas the total level of STAT5a remains relatively constant in treated vs. untreated control, demonstrating the utility of the Total ELISA kits as controls.

four hours. All phosphoELISA™ Kits are rigorously tested to ensure excellent quality. Validation studies include experiments to verify parallelism between calibrated standards and natural samples (Figure 1), peptide competition and cross-reactivity tests for specificity (Figures 2 and 3), and stimulation experiments to ensure correct activation patterns (Figure 4). Specifications include excellent precision (<10% CV), recovery (85–108%), and sensitivity (at least 2× more sensitive than western blots). phosphoELISA™ Kits can be combined with western blot images of specific protein bands to ensure confidence in your results (Figure 5).

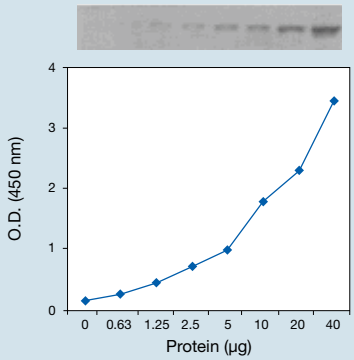

Figure 5—Confirm western data. In parallel, cell extracts were prepared and analyzed with western blots and phosphoELISA™ kits for STAT5 [pY694]. The O.D. reading corresponds to the intensity of the bands in the western blot.

Completely optimized phosphoELISA™ Kits are supplied ready to use with all the necessary reagents, including recombinant standards to be used as positive controls and for quantitative results. In addition, the flexible 96-stripwell plate format allows you to run as many samples, or as few, as you need. For complete information on the Invitrogen™ tools available for studying the JAK-STAT pathway, visit **www.invitrogen.com/pelisa** . ■

References

1. Ihle, J.N. (1996) *Cell* 84(3):331–334.
2. Murray, P.J. (2007) *J Immunol* 178:2623–2629.

Product	Species	Quantity	Cat. no.
Antibodies			
JAK/STAT Sampler	Hu	2 blots	44-429G
JAK1	Hu	100 µg	AHO1512
JAK2 (mAb)	Hu, Ms, Rt	100 µg	AHO1352
STAT3	Hu, Ms, Rt	100 µg	AHO1252
STAT4 (mAb)	Hu, Ms, Rt	100 µg	AHO1342
STAT5 (mAb)	Hu, Ms	100 µg	AHO1462
STAT6 (mAb)	Hu, Ms, Rt	100 µg	AHO1452
phosphoELISA™ kits			
STAT1 [pY701]	Hu	96 tests	KHO0271
STAT1 (Total)	Hu	96 tests	KHO0261
STAT3 [pY705]	Hu, Ms, Rt	96 tests	KHO0481
STAT3 (Total)	Hu, Ms, Rt	96 tests	KHO0471
STAT5a [pY694]	Hu	96 tests	KHO0761
STAT5a (Total)	Hu	96 tests	KHO0751
STAT6 [pY641]	Hu	96 tests	KHO0801
Luminex® assays			
STAT1 (Total)	Hu	96 tests	LHO0261
STAT1 [pY701]	Hu	96 tests	LHO0271
STAT3 [pY705]	Hu, Ms, Rt	96 tests	LHO0481

Fluorescent calcium indicators for *in vivo* imaging of neuronal networks

IMAGES FROM DEEP WITHIN THE NERVOUS SYSTEM.

The development of techniques to visualize functional neuronal activity in the living brain is a key goal of many neuroscientists. In neurons, intracellular calcium plays a critical role during induction of synaptic activity and activation of various signaling pathways. Functional imaging of calcium as a measure of neuronal activity has been aided by Molecular Probes® fluorescent calcium indicators. Until recently, fluorescent methods for calcium imaging were limited to isolated neuronal preparations or brain slices; however, the development of two-photon fluorescence imaging capabilities has allowed neuroscientists to image calcium in neurons buried deep within the living nervous system. Expansion of two-photon *in vivo* imaging has led researchers to develop several novel methods for successful delivery of fluorescent calcium indicators to subsurface layers of the brain, allowing greater access to functional neuronal imaging experiments.

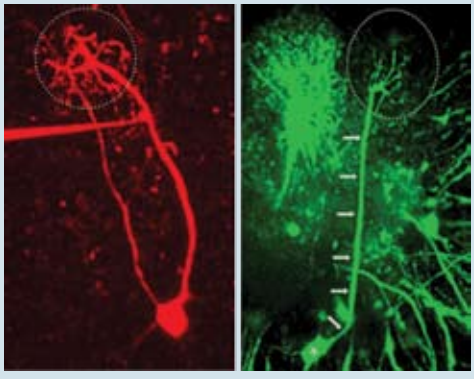

Figure 1—*In vivo* calcium-dye imaging of mitral cell function in the mouse olfactory bulb. Left panel, intracellular staining of a recorded mitral cell with X-rhod-1 potassium salt. The pipette recording site was located at the apical primary dendrite. Right panel, local electroporation with Oregon Green® 488 BAPTA-1 dextran conjugates (10,000 MW) labeled many neuronal processes and allowed the dendritic projection of a mitral cell from the soma (indicated by an asterisk) to be traced to a single olfactory glomerulus (indicated by a white dashed circle). Image contributed by Shin Nagayama and Wei R. Chen.

The challenges of conventional dye-loading methods

Delivery of calcium indicators to neurons *in vivo* was initially achieved through microinjection of salt and dextran forms of fluorescent calcium indicators directly into single neurons.[1–4] While useful for the visualization of calcium signaling in fine neuronal processes, this method is ineffective for the study of neuronal networks because only a single neuron is labeled, dye diffusion is slow, and the injection procedure is invasive. As an alternative, cell-permeant AM ester dyes, including a wide variety of calcium indicators, were initially developed as a simple method for fluorescent dye delivery into cells and tissues. AM esters neutralize the charges of fluorescent dyes and indicators, allowing passive diffusion into live cells; intracellular esterases convert the indicator into a cell-impermeant dye that is retained inside the cell. Neuroscience researchers have used cell-permeant AM esters to deliver fluorescent calcium indicators to a large population of cells in the living nervous system, [5–12] and have been able to monitor neuronal network activity in distinct regions of the brain as well as the spinal cord.[13,14]

A new method for the study of neuronal networks

In a recent issue of *Neuron*, Chen and colleagues published a novel method for fluorescent calcium indicator delivery to the living brain, which combines some of the benefits of single-cell injection and AM ester bulk loading.[15] After injection of fluorescent calcium indicator salts or dextran conjugates to a local brain region, they use electroporation, or short pulses of electrical activity, to transiently disrupt neuronal membranes. Electroporation results in short-lived pores in neuronal membranes, allowing cell-impermeant fluorescent calcium indicators to enter cells in a distinct region. This method of delivery, previously used to load calcium indicators into the spinal cord,[16] results in bright, uniform neuronal labeling of a localized population of neurons within a few hours (Figure 1), enabling better resolution in the analysis of calcium activation in dendritic spines and at

Table 1—Fluorescent calcium indicators used for two-photon *in vivo* imaging of neuronal networks.

Dye	Loading technique	Region of nervous system	Reference	Cat. no.
Calcium Green™-1, AM	AM ester bulk loading	Mouse barrel cortex	Stosiek (2003)	C3011MP, C3012
Oregon Green® 488 BAPTA-1, AM	AM ester bulk loading	Mouse barrel cortex	Stosiek (2003)	O6807
Fluo-4, AM	AM ester bulk loading	Mouse barrel cortex	Stosiek (2003)	F14201
Fura Red™, AM	AM ester bulk loading	Mouse barrel cortex	Stosiek (2003)	F3021, F3022
Calcium Green™-1, AM	AM ester bulk loading	Zebrafish larval spinal cord	Brustein (2003)	C3011MP, C3012
Magnesium Green™, AM	AM ester bulk loading	Zebrafish larval spinal cord	Brustein (2003)	M3735
Indo-1, AM	AM ester bulk loading	Zebrafish larval spinal cord	Brustein (2003)	I1203, I1223, I1226
Oregon Green® 488 BAPTA-1, AM	AM ester bulk loading	Rat cerebellar cortex	Sullivan (2005)	O6807
Fluo-4, AM	AM ester bulk loading	Rat cortical astrocytes	Hirase (2004)	F14201
Oregon Green® 488 BAPTA-1, AM	AM ester bulk loading	Rat cortex	Kerr (2005)	O6807
Rhod-2, AM	AM ester bulk loading	Zebrafish olfactory bulb	Li (2005)	R1244, R1245MP
Oregon Green® 488 BAPTA-1, AM	AM ester bulk loading	Rat visual cortex, cat visual cortex	Ohki (2005, 2006)	O6807
Calcium Green™-1 dextran, 3,000 MW	Electroporation	Mouse spinal cord	Bonnot (2005)	C6765
Calcium Green™-1, salt	Electroporation	Mouse spinal cord	Bonnot (2005)	C3010MP
Oregon Green® 488 BAPTA-1 dextran, 10,000 MW	Electroporation	Mouse olfactory bulb, mouse barrel cortex	Nagayama (2007)	O6798
Calcium Green™-1 dextran, 3,000 and 10,000 MW	Electroporation	Mouse cerebellum	Nagayama (2007)	C6765, C3713
Calcium Green™-1, salt	Electroporation	Mouse cerebellum	Nagayama (2007)	C3010MP
Oregon Green® 488 BAPTA-1, salt	Electroporation	Mouse cerebellum	Nagayama (2007)	O6806

axon terminals. Although the region of labeling is not as extensive as can be obtained with the AM ester bulk loading method, electroporation of fluorescent dextran indicator conjugates allows calcium imaging of several neurons in a local network with enhanced resolution, which can be used to visualize functional neuronal activity at the level of single synapses.

In vivo two-photon imaging and delivery of fluorescent calcium indicators to populations of neurons through AM ester bulk loading or electroporation of cell-impermeant indicators both offer new ways for researchers to assemble information about how neurons function as a network. Both methods have been successfully used to deliver a variety of indicators to several regions of the living central nervous system for examination of neuronal circuit activation during processing of odor and somatosensory stimuli (Table 1). Each technique offers distinct advantages. AM ester bulk loading allows delivery of indicators to a large population of neurons and other cell types in the nervous system, which has allowed researchers to visualize extensive network interactions and signaling, as well as to further characterize calcium signaling in nonneuronal cells such as astrocytes.[5,8,17] On the other hand, electroporation of cell-impermeant indicators results in less extensive labeling and lower background, giving improved resolution of calcium levels in neuronal projections and fine structures.[17]

Tools for tomorrow's neurobiology research

Although calcium indicators have primarily been applied to *in vivo* imaging of anesthetized animals, new two-photon imaging systems are allowing researchers to visualize calcium in the nervous system in awake, freely moving animals without the invasiveness of typical electrophysiological techniques and with easier and faster delivery than genetically expressed fluorescent protein calcium sensors. Molecular Probes® AM ester, salt, and dextran fluorescent calcium indicators, available in a range of fluorescent colors and calcium affinities, are vital tools for the emerging area of *in vivo* functional neuronal imaging. ■

References

1. O'Donovan, M.J. et al. (1993) *J Neurosci Methods* 46:91–106.
2. Svoboda, K. et al. (1997) *Nature* 385:161–165.
3. Helmchen, F. et al. (1999) *Nat Neurosci* 2:989–996.
4. Kreitzer, A.C. et al. (2000) *Neuron* 27:25–32.
5. Stosiek, C. et al. (2003) *Proc Natl Acad Sci U S A* 100:7319–7324.
6. Sullivan, M.R. et al. (2005) *J Neurophysiol* 94:1636–1644.
7. Brustein, E. et al. (2003) *Pflugers Arch* 446:766–773.
8. Hirase, H. et al. (2004) *Biol* 2:E96.
9. Kerr, J.N. et al. (2005) *Proc Natl Acad Sci U S A* 102:14063–14068.
10. Li, J. et al. (2005) *J Neurosci* 25:5784–5795.
11. Ohki, K. et al. (2005) *Nature* 433:597–603.
12. Ohki, K. et al. (2006) *Nature* 442:925–928.
13. Garaschuk, O. et al. (2006) *Pflugers Arch* 453:385–396.
14. Garaschuk, O. et al. (2006) *Nat Protoc* 1:380–386.
15. Nagayama, S. et al. (2007) *Neuron* 53:789–803.
16. Bonnot, A. et al. (2005) *J Neurophysiol* 93:1793–1808.
17. Helmchen, F. and Nevian, T. (2007) *Neuron* 53:771–773.

Product	Quantity	Cat. no.
Oregon Green® 488 BAPTA-1, AM	10 x 50 µg	O6807
Calcium Green™-1, AM	500 µg	C3011MP
Calcium Green™-1, AM	10 x 50 µg	C3012

O-GlcNAc: Hiding in plain sight

CLEVER CHEMISTRY REVEALS AN ENIGMA OF GLYCOBIOLOGY.

The *O*-GlcNAc (*O*-linked β-*N*-acetylglucosamine) modification is an abundant, highly dynamic, intracellular regulatory modification found in all eukaryotic cells; like phosphorylation, *O*-GlcNAc modification significantly alters target protein function.[1] This modification occurs on serine and threonine residues, and a complex relationship has been proposed between *O*-GlcNAc and *O*-phosphate, involving both competitive and additive effects.[2] In addition to its roles in signaling and protein expression, degradation, and turnover, *O*-GlcNAc is emerging as a key modification in the progression of several important disease states, including diabetes, Alzheimer's disease, and cancer, as well as a general modification in response to stress.

Why *O*-GlcNAc is such a mysterious modification

The *O*-GlcNAc modification presents several formidable challenges for its detection. First, it is a very small, uncharged molecule—as a result, *O*-GlcNAc–modified proteins migrate no differently from unmodified ones. Additionally, it is often present at very low levels, beyond the detection limits of antibody- and lectin-based methods. Finally, *O*-GlcNAc is very labile; even with mass spectrometry, the molecule is often lost—until now.

New tools to detect this previously elusive molecule

Invitrogen now offers researchers two novel tools to label *O*-GlcNAc–modified proteins either metabolically or enzymatically and to detect *O*-GlcNAc at femtomole levels (Figure 1) in gels or western blots with a method that is also mass spectrometry–compatible for protein identification. For metabolic labeling, cultured cells are incubated with the Click-iT™ GlcNAz metabolic glycoprotein labeling reagent. The azido-modified sugar is then metabolically incorporated into a protein through the permissive nature of the oligosaccharide biosynthesis pathway, yielding a glycoprotein containing the Click-iT™ azide handle. Pure proteins, cell lysates, or protein extracts thought to contain

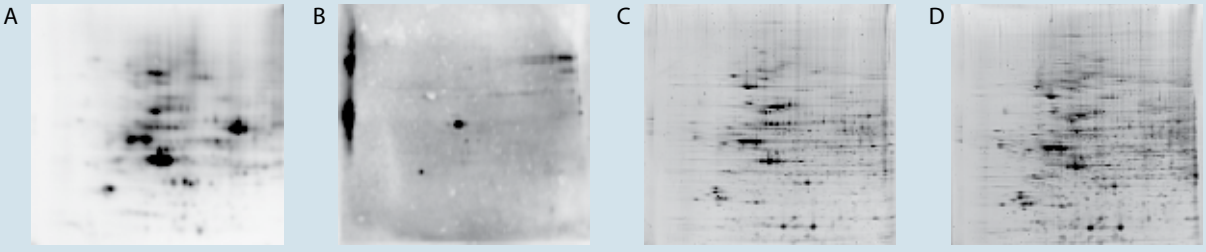

Figure 1—Comparison of Click-iT™ metabolic detection of *O*-GlcNAc–modified glycoproteins with antibody-based detection. (A) Jurkat cells were metabolically labeled with Click-iT™ GlcNAz metabolic glycoprotein labeling reagent, followed by biotinylation of the GlcNAz-labeled proteins with the Click-iT™ Biotin Glycoprotein Detection Kit. Twenty milligrams of cell extract were separated on pH 4–7 IEF strips followed by NuPAGE® gel electrophoresis, then blotted to PVDF membrane. Biotinylated *O*-GlcNAc glycoproteins were visualized with a streptavidin–horseradish peroxidase (HRP) conjuagte. (B) 2D western blot of 40 mg unlabeled Jurkat cell extract separated and blotted as in (A), then visualized with the anti–*O*-GlcNAc antibody CTD110.6, followed by the HRP conjugate of goat anti–mouse IgG antibody. In (A) and (B), HRP detection was performed using the protocols and reagents provided in the Pierce *O*-GlcNAc detection kit. The left marker lane in (B) contains 5 ng of *O*-GlcNAc bovine serum albumin (BSA) positive control from the Pierce kit. (C) Gel of sample (A) stained with SYPRO® Ruby total protein stain. (D) Gel of sample (B) stained with SYPRO® Ruby total protein stain.

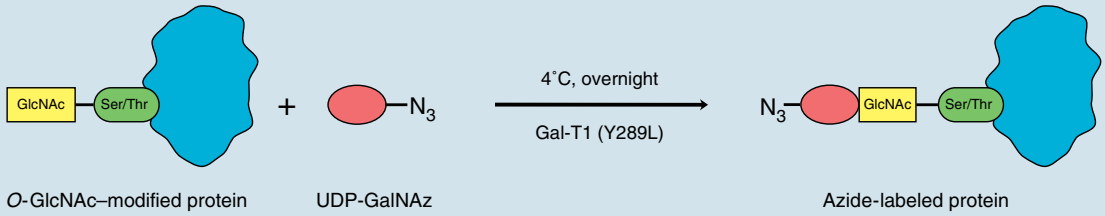

Figure 2—Enzymatic labeling of an *O*-GlcNAc–modified glycoprotein with UDP-GalNAz and the permissive mutant β-1,4-galactosyltransferase (Gal-T1 (Y289L)).

Table 1—Compatibility of the Click-iT™ Glycoprotein Detection Kits with other methods.

		Compatibility with detection methods			Spectral compatibility with Multiplexed Proteomics® stains		
Kit	Cat. no.	1D or 2D gel	Western blot	Mass spectrometry	SYPRO® Ruby protein gel stain	Pro-Q® Emerald glycoprotein gel stain	Pro-Q® Diamond phosphoprotein gel stain
Click-iT™ Tetramethylrhodamine (TAMRA) Glycoprotein Detection Kit	C33370	•	•*	•	•	•	
Click-iT™ Dapoxyl® Glycoprotein Detection Kit	C33371	•		•	•		•
Click-iT™ Biotin Glycoprotein Detection Kit	C33372		•	•			

* Western detection requires an anti-tetramethylrhodamine antibody (e.g., Invitrogen Cat. no. A6397).

O-GlcNAc–modified proteins can be enzymatically labeled with the Click-iT™ *O*-GlcNAc Enzymatic Labeling System. *O*-GlcNAc–modified glycoproteins are enzymatically labeled with the Click-iT™ azide handle by utilizing the permissive mutant β-1,4-galactosyltransferase (Gal-T1 (Y289L)), which transfers azide-modified galactosamine (GalNAz) from UDP-GalNAz to *O*-GlcNac residues on the target proteins (Figure 2). Once the proteins are labeled, detection is achieved using "click" chemistry—a copper-catalyzed reaction between an azide and an alkyne. There are three different Click-iT™ Glycoprotein Detection Kits (Table 1), which provide either a fluorescent or biotinylated azide-reactive alkyne along with the necessary click reaction components. Detecting *O*-GlcNAc is now a simple and robust two-step process.

O-GlcNAc in context

The Click-iT™ method offers the potential to multiplex with other detection technologies, permitting an unprecedented characterization of cellular posttranslational modifications. Used in combination with Multiplexed Proteomics® technologies, Click-iT™ glycoprotein profiling reagents allow researchers to detect *O*-GlcNAc together with total protein, total glycoprotein, or total phosphoprotein, all in the same gel (Table 1). They are also compatible with multiplexed western blots and mass spectrometry. Their sensitivity and compatibility will be critical in helping to elucidate the biological relevance of this posttranslational modification as well as its relationship with phosphorylation of serine and threonine residues on key regulatory proteins.[3,4] ■

References

1. Wells, L. and Hart, G.W. (2003) *FEBS Letters* 546:154–158.
2. Hart, G.W. et al. (2007) *Nature* 446:1017–1022.
3. Halling, D.B. et al. (2005) *Sci STKE* 2005:re15.
4. Slawson, C. et al. (2006) *J Cell Biochem* 97:71–83.

Product	Quantity	Cat. no.
Click-iT™ GlcNAz Metabolic Glycoprotein Labeling Reagent (tetraacetylated *N*-azidoacetylglucosamine), for *O*-GlcNAc–modified proteins	5.2 mg	C33367
Click-iT™ *O*-GlcNAc Enzymatic Labeling System, for *O*-linked GlcNAc glycoproteins, 10 labelings	1 kit	C33368
Click-iT™ Tetramethylrhodamine (TAMRA) Protein Analysis Detection Kit, UV/532 nm excitation, 10 reactions	1 kit	C33370
Click-iT™ Dapoxyl® Protein Analysis Detection Kit, for UV excitation, 10 reactions	1 kit	C33371
Click-iT™ Biotin Protein Analysis Detection Kit, 10 reactions	1 kit	C33372
anti-tetramethylrhodamine, rabbit IgG fraction	0.5 mL	A6397

FAST AND EASY PROFILING WITH LUMINEX® TRANSCRIPTION FACTOR ASSAY KITS

The Luminex® Transcription Factor Assay Kits provide a faster, less labor-intensive method for assessing transcription factors' DNA-binding capabilities within a cell nucleus. By taking advantage of the Luminex® xMAP® platform, a technology that combines the sensitivity of flow cytometry and digital signal processing with the speed and flexibility inherent in a liquid bead array approach, you can achieve complete profiling of 20 transcription factors at once, or more targeted measurement of specific transcription factors.

- Profile up to 20 transcription factors in one assay
- Save time with a 90 minute assay
- Confirm gel shift results and publish

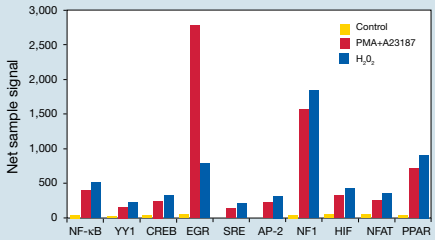

Induction of transcription factors in THP-1 cells. Differential expression of 10 transcription factors in response to treatment with PMA or hydrogen peroxide when measured simultaneously using Invitrogen's multiplex kits for Luminex® xMAP® technology.

Below are a few of the Luminex® Transcription Factor Assay Kits we offer. Find the complete list at **www.invitrogen.com/luminex**.

Product	Quantity	Cat. no.
AP2	100 rxns	LHF0021
CREB	100 rxns	LHF0051
EGR	100 rxns	LHF0081
HNF-1	100 rxns	LHF0101
NF-κB	100 rxns	LHF0151
NF-1	100 rxns	LHF0141
PPAR	100 rxns	LHF0171
YY1	100 rxns	LHF0201

xMAP® is a registered trademark of Luminex Corporation.

OMNIA™ IP KINASE ASSAYS FOR REAL-TIME DATA

Tired of radioactivity? Now you can get the same reliability as radioactive filter-binding assays—without the hazardous material and with some additional advantages—using the Omnia™ IP kinase assays. Omnia™ IP kinase assays (agarose bead or plate format) use a specific monoclonal or polyclonal antibody to capture the target of interest from a complex mixture of proteins in crude cell lysate. The kinase activity of the captured target is then measured in real time, giving you highly specific kinetic data.

- Kinetic results from real-time data
- Safe and easy method, no radioactivity
- Accurate information from specific kinase activity measurements

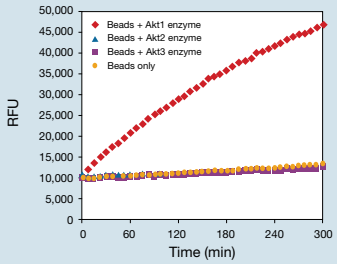

Specificity. The Omnia™ IP kinase assay for Akt1 showed activity for only Akt1, and not Akt2 or Akt3, illustrating the selectivity conferred by the monoclonal antibody used to capture Akt1 from the cell lysate.

See some of the Omnia™ IP kinase assays below. For a complete list of specificities visit us at **www.invitrogen.com/omnia**.

Product*	Quantity	Cat. no.
Omnia™ Plate IP Kits		
B-Raf	96 rxns	KNZ7011
p38 MAPK	96 rxns	KNZ7041
Omnia™ Agarose Bead IP Kits		
Akt1	40 rxns	KNZ6011
ERK1&2	40 rxns	KNZ6031
p70-S6K	40 rxns	KNZ6051

* Omnia™ Plate IP Kits include substrate peptide, phosphopeptide control, ATP solution, DTT solution, kinase reaction buffer, antibody-coated 96-well plate, cell lysis buffer, inactive kinase mix, adhesive plate cover strips, and wash buffer. Omnia™ Agarose Bead IP Kits include substrate peptide, phosphopeptide control, ATP solution, DTT solution, kinase reaction buffer, cell lysis buffer, antibody solution, protein A and G agarose beads, and wash buffer.

ANTIBODIES FOR NEURODEGENERATION AND NEUROTRANSMITTER STUDIES

Invitrogen is well known for high-quality research tools for the study of neurodegenerative disorders such as Alzheimer's and Parkinson's diseases. Expanding on a broad menu of antibodies and assays for tau, β amyloid, and α-synuclein research, Invitrogen now offers antibodies for studying neurotransmitter signaling pathways.

- Reagents for Alzheimer's, Parkinson's, memory, and substance abuse research

- Antibodies for GABA, NMDAR, and splice variants
- Antibodies for neurotransmitter signaling pathways

Here are just a few of the more than 300 antibodies Invitrogen offers for neurobiology research. View them all at **www.invitrogen.com/antibodies/neuroscience**. To keep up to date with all new antibody releases, check back often at **www.invitrogen.com/antibodies**.

Product	Reactivity *	Applications †	Quantity	Cat. no.
GABAA Receptor a1 (N-term)	Ms, Rt, B, C, Hu	WB	100 µl	48-3900
NMDA NR1 (Variant C1)	Ms, Rt, B, C, Hu	WB	25 µg	48-4800
NMDA NR1 (Variant C2′)	Ms, Rt, B, Hu	WB	25 µg	48-6500
GABAA Receptor a4, (N-term)	Rt	WB	100 µl	48-4100
v-Ras (mAb)	Hu, Ms, Rt	WB, IP, IF, IHC	50 µg	33-7200
α-CaM Kinase II (mAb)	Hu, Ms, Rt, Ov, Gf	WB, E, IP, IHC	100 µg	13-7300

* Gf = goldfish, C = canine, B = bovine, Hu = human, Ms = mouse, Ov = ovine, Rt = rat; † E = ELISA, IF = immunofluorescence, IHC = immunohistochemistry, IP = immunoprecipitation, WB = western blot. All antibodies are polyclonal unless stated otherwise.

BIOSOURCE™ IL-23 HETERODIMER ELISA KITS FOR CONSISTENT, ACCURATE DATA

BioSource™ ELISA kits deliver relevant data from minimal sample quantities so you can get the complete story from both inside and outside the cell. Each kit contains NIBSC-calibrated recombinant standards for quantification, and highly specific antibody pairs for the target protein. Rigorous quality control testing ensures that you produce reliable results with no lot-to-lot variations.

- Sensitive measurements, down to picogram levels
- Specific detection of the target protein of interest without crosstalk
- Easy-to-follow protocols and essentials always included

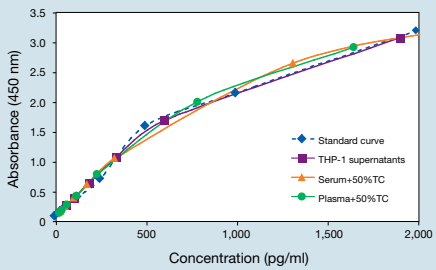

Parallelism between recombinant and natural Hu IL-23. The optical densities of dilutions of THP-1 cell supernatants (stimulated with IFN-γ and infected with *E. coli*), and human serum and plasma spiked with natural Hu IL-23 heterodimer, were plotted alongside Hu IL-23 standards. The parallelism indicates that the standard accurately reflects the Hu IL-23 heterodimer content in natural samples.

Here are a few of the hundreds of BioSource™ cytokine and signaling ELISAs available from Invitrogen. To see them all, learn more about the technology, or to place your order, visit **www.invitrogen.com/elisa**.

Product	Quantity	Cat. no.
Human IL-23 Heterodimer ELISA Kit	96 tests	KHC0231
Human IL-23 Heterodimer ELISA Kit	192 tests	KHC0232
Mouse IL-23 ELISA Kit	96 tests	KMC0231
Mouse IL-23 ELISA Kit	192 tests	KMC0232

AMPLIFY WEAK GFP SIGNALS IN FIXED CELLS AND TISSUES

Invitrogen's anti-GFP rabbit polyclonal antibody is raised against Green Fluorescent Protein (GFP) isolated directly from *Aequorea victoria*, and is available as a complete antiserum or as an IgG fraction purified by ion-exchange chromatography. This antibody is suitable for immunoprecipitation or for detection of native GFP, GFP variants, and most GFP fusion proteins by western blot analysis.

- Amplify weak GFP signals
- Detect native GFP, GFP variants, and most GFP fusions
- Useful for western blots, IHC, ICC, and immunoprecipitation

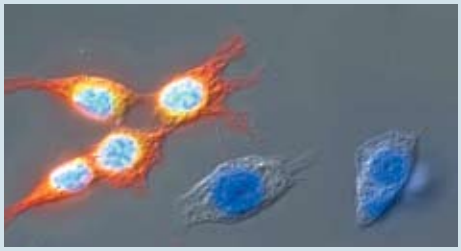

Bright GFP expression. NIH 3T3 cells (transiently transfected with a GFP expression vector) were fixed and labeled with the Alexa Fluor® 594 conjugate of the anti-GFP antibody. About 10% of the cells were expressing GFP and show dual labeling of both GFP and the anti-GFP antibody (green and red fluorescence overlap to yield yellow). Blue-fluorescent DAPI stains the nuclei, and in nontransfected cells the DAPI stain is the only fluorescence signal seen.

Learn more at **www.invitrogen.com/antibodies**.

Product	Quantity	Cat. no.
anti-GFP, rabbit serum	100 µl	A6455
anti-GFP, IgG fraction	100 µl	A11122
anti-GFP, IgG, Alexa Fluor® 488 conjugate	100 µl	A21311
anti-GFP, IgG, Alexa Fluor® 555 conjugate	100 µl	A31851
anti-GFP, IgG, Alexa Fluor® 594 conjugate	100 µl	A21312
anti-GFP, IgG, Alexa Fluor® 647 conjugate	100 µl	A31852

Recently published

A LOOK AT HOW YOUR COLLEAGUES ARE USING INVITROGEN™ PRODUCTS.

Qdot® nanocrystals enable simultaneous *in vivo* imaging of lymphatic basins. Researchers from the National Cancer Institute report the use of multicolored quantum dot nanocrystals (Qdot® 565, Qdot® 605, Qdot® 655, Qdot® 705, and Qdot® 800 ITK carboxyl quantum dots) and spectrally resolved *in vivo* imaging to simultaneously visualize up to five lymphatic drainage basins in mice. This constitutes an advance over existing X-ray, magnetic resonance, or radionuclide lymphangiography techniques, which require sequential analysis in order to differentiate the contributions from each lymphatic basin.

Kobayashi, H., Hama, Y., Koyama, Y., Barrett, T., Regino, C.A., Urano, Y., Choyke, P.L. (2007) Simultaneous multicolor imaging of five different lymphatic basins using quantum dots. *Nano Lett* 7:1711–1716.

Reactive oxygen species–dependent transcription factor expression. Generation of reactive oxygen species (ROS) over the course of 12 hours following ultraviolet irradiation of primary human keratinocytes exhibits a biphasic time dependence. Using the fluorescent ROS sensors CM-H_2DCFDA and MitoSOX™ Red mitochondrial superoxide indicator, Rezvani and coworkers show that the early and late phases of ROS generation derive from cytoplasmic and mitochondrial sources, respectively, and produce different effects on the expression of the oxygen-sensitive transcription factor HIF-1.

Rezvani, H.R., Dedieu, S., North, S., Belloc, F., Rossignol, R., Letellier, T., de Verneuil, H., Taieb, A., Mazurier, F. (2007) Hypoxia-inducible factor-1alpha, a key factor in the keratinocyte response to UVB exposure. *J Biol Chem* 282: 16413–16422.

Structural and functional analysis of MRP1 multidrug resistance transporter. Differences between Jurkat and Raji lymphocytes in the extent of glutathione release during apoptosis can be ascribed to the MRP1 multidrug resistance transporter, according to researchers at the University of Rochester. They used calcein AM microplate assays to assess functional activity of MRP1 and analyzed its cellular localization by confocal microscopy using Alexa Fluor® 647 dye–labeled secondary antibodies in combination with FIX & PERM® reagents and FM® 1-43FX and SYTOX® Green nucleic acid stain for plasma membrane and nuclear labeling, respectively.

Hammond, C.L., Marchan, R., Krance, S.M., Ballatori, N. (2007) Glutathione export during apoptosis requires functional multidrug resistance-associated proteins. *J Biol Chem* 282:14337–14347.

Underlying molecular mechanisms of viral membrane fusion. Thiol-reactive probes and membrane fusion assays were among the tools employed by researchers at the University of Massachusetts Medical School to analyze the role of protein thiol/disulfide exchange in Newcastle disease virus (NDV) infection. Viral infection of COS-7 cells was monitored by immunofluorescence microscopy using rabbit anti-NDV antibodies in combination with Alexa Fluor® 488 dye–labeled secondary antibodies. The extent of hemifusion between infected COS-7 cell membranes and red blood cell membranes was assessed using the lipid tracer octadecyl rhodamine B. The membrane-impermeant reagent N^{α}-(3-maleimidylpropionyl)biocytin was used to selectively biotinylate free thiols on cell-surface proteins for subsequent precipitation and western blot analysis.

Jain, S., McGinnes, L.W., Morrison, T.G. (2007) Thiol/disulfide exchange is required for membrane fusion directed by the Newcastle disease virus fusion protein. *J Virol* 81:2328–2339.

Drug-induced phospholipidosis assay validation. A comparison of biomarker gene expression analysis and fluorescence-based phenotype detection methods for assessment of drug-induced phospholipidosis has been conducted by a team from the Schering-Plough Research Institute. Fluorescence assays using HepG2 cells and the HCS LipidTOX™ Red phospholipidosis detection reagent correctly identified 100% of 24 known phospholipidosis-positive and -negative compounds. They conclude that the fluorescence assay is less time consuming, more sensitive, and capable of higher sample throughput than gene expression analysis.

Nioi, P., Perry, B.K., Wang, E.J., Gu, Y.Z., Snyder, R.D. (2007) In vitro detection of drug-induced phospholipidosis using gene expression and fluorescent phospholipid based methodologies. *Toxicol Sci* 99:162–173.

The publications summarized here are just a few of the recent additions to the 59,000+ references describing applications of Molecular Probes® products in our searchable bibliography database at **probes.invitrogen.com/servlets/bibsearch**.

WANT TO SEE YOUR NAME ON THIS PAGE?
Send your bibliographic references featuring Invitrogen™ products to **bioprobes@invitrogen.com**.